I.Kubin, T. O. Zörner, L. Gardini and P. Commendatore, A credit cycle model with market sentiments, Structural Change and Economic Dynamics 50 (2019) 159 -174. https://doi.org/10.1016/j.strueco.2019.06.006

A credit cycle model with market sentiments

Ingrid Kubin[a]*, Thomas O. Zörner[a],
Laura Gardini[b], and Pasquale Commendatore[c]
[a]Vienna University of Economics and Business Administration, Austria,
[b]University of Urbino, Italy,
[c]University of Naples Federico II, Italy

Abstract

This paper extends Matsuyama's endogenous credit cycle model to account for recent findings on the role of credit market sentiments. The benchmark model uses a parsimonious financial friction specification in the form of a pledgeability parameter, which indicates how much of the revenue borrowers can pledge for credit. We endogenize this parameter by introducing behavioral aspects of credit markets. Depending on the current level of net worth the credit market sentiment may change. If a critical net worth threshold is passed, a switch from an optimistic to a pessimistic regime occurs. Lenders' perception of risk and the pledgeability parameter will vary accordingly. The resulting dynamic law of motion is two-dimensional and discontinuous. We show that switching between beliefs fundamentally affects the stability of the system confirming that changes in credit market sentiments drive volatility. However, we also find instances in which behavioral regime switches have a stabilizing effect.

Keywords: Credit Cycles, Financial Frictions, Market Sentiments, Behavioural Inertia

JEL Codes: E32, E44, G41.

*Corresponding author: ingrid.kubin@wu.ac.at.

1 Introduction

In a recent contribution, López-Salido et al. (2017) classify the theories of credit cycles, grouping them into two broad categories. The first category introduces credit market imperfections into dynamic stochastic general equilibrium models that are based on rational agents and perfect markets. For example, in their pioneering work, Kiyotaki and Moore (1997) assume that borrowers' access to credit is limited by the value of some collateralized asset, which varies endogenously. In Bernanke and Gertler (1989), imperfect financial markets are a consequence of asymmetric information between borrowers and lenders such that external finance is more costly than internal finance. This cost difference depends upon the balance sheet position of the borrower (more specifically, upon the borrower's net worth), that, through its own dynamics, might interact with the business cycle. A vast branch of literature involving balance sheet measures emerged from the above mentioned seminal contributions (Favara 2012, Schularick and Taylor 2012, Baron and Xiong 2017, inter alia). In these models, the explanation of business cycles rests to a large extent on exogenous stochastic shocks. Financial frictions and other mechanisms amplify, propagate or absorb these shocks, but they are not an endogenous source of fluctuations.

The second classification collects approaches that assign a crucial role to investor sentiments. This includes behavioral theories that relate to Minsky's financial fragility hypothesis (Minsky, 1982), animal spirits[1] or psychological research, often introduce some elements of irrationality or assume bounded rationality. For example, Bordalo et al. (2018) and more broadly Gennaioli and Shleifer (2018) provide ample empirical evidence on the effects of variations in risk perceptions and default probabilities and thus corroborate the behavioral view on credit cycles that does not rely on balance sheet measures. The main feature of their model concerns the importance of agents' (subjective) belief formation. Following Kahneman and Tversky (1972), they implemented a formalization of the so-called "representativeness" heuristic where beliefs are formed in a way such that agents extrapolate a general trend from the most recent performances of a variable. Subsequently, this leads to an overestimation of the probability of continuing the past performance leading to excessive optimism or pessimism. Employed in a credit cycle model, Bordalo et al. (2018) are able to show that "diagnostic expectations" based on above mentioned heuristic lead to excessive volatility of credit spreads due to an overreaction to new information compared to belief formation under rational expectations. Hence, they provide a model based on a psychological based belief formation which is able to reproduce stylized facts of credit market behavior in an endogenous setting.

Another endogenous explanation of credit cycles was provided by Matsuyama (2013) and Matsuyama et al. (2016). While the authors acknowledge that their process resembles Minsky's mechanism, they clearly view their explanation as an alternative since "[t]he model [...] does not rely on any form of irrationality" (Matsuyama et al., 2016, p. 528). By using a straightforward and parsimonious specification, in the spirit of Tirole's (2005) pledgeability approach for modeling financial frictions, cycles emerge endogenously. In a nutshell, the model framework and the structure of their analysis are the following.[2] In an overlapping generations framework, agents accumulate net worth (consisting of wage income) in one period and at the beginning of the next period they have three investment options, in which they can allocate their net worth: Good projects, Bad projects and Lending. Good projects, involving investments in the production of goods, generate a pecuniary externality by driving up next generation agents' net worth through a rise in labor demand; whereas Bad projects, involving a simple transformation of the final good without generating labor demand, do not imply any intergenerational spillover effect, need finance and are subject to credit rationing.

These ingredients are sufficient to generate cycles through the following mechanism. Starting with a low net worth, only investments in Good projects are feasible due to a binding borrowing constraint. The stock of productive capital therefore increases which in turn rises the wage rate and thus also the net worth (which eases the borrowing constraint), while the marginal product of capital declines (which makes Good projects less attractive). With an easing borrowing constraint, agents can now start investing in Bad projects. As resources are moved away from Good projects, the physical capital stock declines. The marginal product of

[1] According to Keynes, animal spirits are defined as "a spontaneous urge to action rather than inaction, and not as the outcome of a weighted average of quantitative benefits multiplied by quantitative probabilities" (Keynes 1936, p.161). For an overview about modeling "animal spirits" in macroeconomic contexts, see Franke and Westerhof (2017).

[2] Matsuyama (2013) puts forward the original specification. Matsuyama et al. (2016) present a streamlined version of this model to focus on the key mechanism behind economic fluctuations and derive analytical details on the properties of these fluctuations under the assumption of a Cobb-Douglas production technology.

labor and the wage rate declines - credit constraints start binding again - and the marginal product of capital increases - Good projects become more attractive again and the cycle starts over. Thus, along this process, where "the Good [projects] breed the Bad [projects] and the Bad [projects] destroy the Good [projects]", the interplay between these different investment options and the specific features of the financial market give rise to endogenous cycles.

Central to this framework are credit market imperfections: lenders will only accept a fraction, labelled μ, of the expected return of the Bad project as collateral for the credit, required to finance Bad projects. According to Matsuyama (2008) the parameter is "meant to capture all sorts of agency problems that restrict the agents' ability to finance the profitable investment externally". Thus, the fraction μ is called *pledgeability parameter* and controls for the strength of agency problems in a very parsimonious way.[3]

López-Salido et al. (2017) thus highlight a dichotomy: the financial friction approach is anchored in the economics' rationality paradigm, but is often insufficient to explain credit cycles endogenously. The behavioral approach departs from this narrow rationality perspective, but it can explain cycles as an endogenous phenomenon. Matsuyama (2013) and Matsuyama et al. (2016) challenge this dichotomy: their approach clearly belongs to the first strand of literature, but it is nevertheless able to explain cycles endogenously. However, this does not discount the relevance of the behavioral approach. López-Salido et al. (2017) and, more generally, the literature on behavioral finance (see López-Salido et al., 2017, and the main literature on behavioral finance, for example, Shleifer, 2000; Thaler, 2003; Shiller, 2003; Nofsinger, 2005; Baker and Wurgler, 2007; Shu, 2010; Gao and Suess, 2015; Hotz-Behofsits et al., 2018; and Bordalo et al., 2018) provide ample empirical evidence on the relevance of credit market sentiments for the explanation of cycles. According to this approach, the business mood may affect credit market sentiments, which in turn impact on financial and economic decisions. Changes in the business mood and switches in credit market sentiments may exacerbate economic fluctuations and magnify volatility.[4]

In this paper, we combine both strands of literature and introduce selected behavioral elements to the Matsuyama (2013) and Matsuyama et al. (2016) model. Within this original framework, agents have a persistent and unique view about the severity of agency problems, summarized by the exogenous pledgeability parameter μ. In our extension, we assume that the *pledgeability ratio* is endogenous and thus may vary through time determined by a simple heuristic rule: agents assess, if the actual net worth w_t – proxying the current state of the economy – lies above or below some threshold value, $\overline{w}$ and reflect this assessment in an optimistic or pessimistic market sentiment, respectively.[5] In our interpretation, this threshold value reflects the psychological state of lenders – which could facilitate (or hamper) changes in the credit market sentiment – representing a subset of the overall business mood. When the lenders mood is good, the value of the threshold is smaller, thus a switch to an optimistic regime is more likely; when their mood is bad, the switch to an optimistic regime is more difficult to achieve.

When optimism is the dominant view, lenders – perceiving agency problems as less severe - are willing to accept a higher share of the future returns as collateral. In contrast, when the pessimistic view prevails, lenders are less confident that the borrowers will repay the credit – perceiving agency problems as quite severe – and thus are willing to accept a relatively small share of future returns as collateral. Thus, depending on the prevailing credit market sentiment, agents may fix a (relatively) low or a (relatively) high pledgeability ratio. We assume that the market is characterized by two "fundamental" opinions about the strength of the agency problems, resulting in two extreme values of the pledgeability ratio, μ_P and μ_O. Furthermore, we assume that agents do not jump abruptly from one fundamental perception of the agency problems to the other, rather, agents gradually adjust towards the optimistic or pessimistic fundamental perception. The pace depends on how strong the past behavior is taken into account. The adjustment process, thus, involves the memory of past perceptions and reflects behavioral inertia.[6] We introduce a further parameter, ζ, that indicates how fast agents move in the direction of the fundamental value of the respective regime.

To summarize: we focus on the role of the perceived agency problems (reflected in the parameters μ_P

[3] For a deeper discussion of agency problems through limited pledgeability of collaterals, see Tirole (2005).

[4] For more empirical oriented studies in a macroeconomic context, we refer to Franke (2008) and Lux (2009) who utilize industrial survey indices, the Ifo Business Climate index and the ZEW index for Economic Sentiment respectively, to capture sentiment changes between pessimistic and optimistic beliefs.

[5] This simple rule resembles the "representativeness" heuristic proposed by Kahneman and Tversky (1972) and it is consistent with the "diagnostic expectations" approach by Gennaioli and Shleifer (2018) and Bordalo et al. (2018).

[6] This approach follows the "conservatism" heuristic of Edwards (1968) where agents assign a low weight to new information when making decisions.

and μ_O), which are subject to change over different credit market sentiments (the likelihood of the change reflected in the parameter $\overline{w}$). Moreover, we analyze the role of the pace of behavioral adjustment (reflected in the parameter ζ) by modeling a regressive process towards the fundamental perception of agency problems.

The baseline framework and our extension do not provide a microfoundation of the above discussed agency problems. However, we explicitly model the behavioral aspects behind the pledgeability ratio and its dynamics. In the original specification, the pledgeability parameter is exogenously fixed and time invariant and therefore unable to capture behavioral phenomena. Our model collapses to the one presented in Matsuyama et al. (2016) when market sentiments do not affect creditors beliefs ($\overline{w} = 0$ or $\overline{w} = 1$) and agents do not update their pledgeability ratio ($\zeta = 1$) or when agents have a unique perception of the agency problems: i.e. if $\mu_O = \mu_P$. To facilitate comparison, we assume that for the baseline model $\overline{w} = 1$ and $\mu = \mu_P$ holds – corresponding to a situation where the pessimistic scenario always prevails and the agency problems are seen as quite severe. Moreover, to highlight the role of the behavioral parameters, we choose a parameter set for which the baseline model exhibits chaotic fluctuations of agents' net worth. We explore two possible departures from this benchmark. The first scenario considers a large difference between the optimistic and pessimistic pledgeability ratio. The second scenario clarifies the implications of a smaller difference.

If a switch to an optimistic regime corresponds to a substantial change in the fundamental value of the pledgeability ratio, we find the following:

- By reducing $\overline{w}$ (allowing for changes in credit market sentiments) a transition occurs from a persistent pessimistic regime with chaotic fluctuations to a switching between pessimistic and optimistic regime with cycles of finite length. This suggests that the consideration of credit market sentiments may stabilize the economy by reducing the more erratic and turbulent fluctuations. However, in situations where periodic cycles occur, fluctuations are amplified. In this sense, credit market sentiments have a destabilizing effect, imposing more significant changes on the economy. This type of destabilizing effect, occurring for intermediate values of $\overline{w}$, is quite robust with respect to different parameter settings. If we reduce $\overline{w}$ further, the fixed point of the agents' net worth becomes stable. Therefore, allowing for an easy switch in favour of the optimistic regime has a stabilizing effect.

- By reducing ζ (adding sluggishness to the adjustment of the pledgeability ratio) and starting from a value of $\overline{w}$ corresponding to regular cycles, we observe a continuous swing between expansions and reductions in the fluctuations' period. Therefore, behavioral inertia adds an additional source of complexity, which has substantial effects regarding the system's predictability. This situation occurs for high and intermediate values of ζ. For small values of ζ, chaotic behavior can be observed (analogous to an increase in $\overline{w}$). In this sense, behavioral inertia has a destabilizing effect, even though it also implies cycles with smaller length.

If a switch to an optimistic regime leads to a small change in the fundamental value of the pledgeability ratio instead, we find the following effects:

- Reducing $\overline{w}$ has similar effects compared to the previous case. It stabilizes the economy's net worth evolution by reducing the more erratic behavior, but it causes wider fluctuations. Given that the pledgeability ratio does not change substantially from the baseline case in both regimes, a small $\overline{w}$ does not eliminate the fluctuations.

- Reducing ζ has predominantly a small influence on the overall dynamics. However, for a non-negligible set of behavioral parameter values (corresponding to intermediate values of $\overline{w}$ and ζ) chaotic fluctuations emerge. Thus, also in this scenario, behavioral inertia has a significant destabilizing effect.

Our findings are in line with Matsuyama (2013) and Matsuyama et al. (2016), where a low pledgeability ratio reflects a high degree of credit market imperfections. Thus, allowing a switch to an optimistic regime, which involves a higher pledgeability ratio, actually reduces credit market imperfections and exerts a stabilizing effect by reducing erratic and turbulent behavior. At the same time, credit market sentiments and behavioral inertia have destabilizing properties that amplify fluctuations and increase volatility. We are therefore able to confirm the findings of the behavioral finance literature.

Moreover, we observe regions where different attractors coexist, which introduce an element of hysteresis to our model and thus has important economic implications. The phenomenon of multistability was also

observed in other economic model (see, for example, Commendatore et al., 2017; Sushko et al., 2018; Campisi et al., 2018; Lamantia and Radi, 2018; Radi and Gardini, 2015). In our context it is of particular interest, since we find coexisting attractors with quite different dynamic properties: an attrator with a rather low frequency and a limited amplitude coexists with a four-piece chaotic attractor with a much higher amplitude. A small transitory shock (for instance, to the pledgeability ratio or to the initial conditions) may thus have a substantial effect on the long-run characteristics of the time series; and a shock of equal size in the opposite direction will not necessarily restore the initial situation. Thus, single exogenous shocks may actually produce time series with volatility clustering, a phenomenon also prevalent in financial markets' time series.

The remainder of the paper is structured as follows. After introducing the model framework in Section 2, we present the map that summarizes the economic model and underlines the dynamic evolution of the system in Section 3. Section 4 is dedicated to the study of the effects of the behavioral parameters on the structure of the model and on the dynamics, by providing both analytical results and economic interpretations. Section 5 concludes the paper.

2 The benchmark model with dynamic friction perceptions

In this section, we provide a concise exposition of the original model as presented in Matsuyama et al. (2016) and extend it by introducing behavioral features as discussed above.

The model adopts an overlapping generations framework (Diamond, 1965) with two period lives and a unit measure of agents. Time is discrete and runs from zero to infinity, $t = 0, 1, 2, ...$ In each period one final good, the numeraire, is produced which can be used for investments or for consumption. The final goods sector uses the following Cobb-Douglas technology

$$Y_t = AK_t^{\alpha} L_t^{1-\alpha},$$

where Y denotes the final commodity (which is also used as numeraire); A is some exogenous total factor productivity; K_t is physical capital (consisting of the final commodity); L_t is labor at time t, and $\alpha < 1$ is the production elasticity. Expressing the variables in "units of labor" and setting $(1-\alpha)A = 1$, which ensures, after suitable boundary conditions are introduced, that the output is normalized between zero and unity, the output is defined as

$$\frac{Y_t}{L_t} = y_t = f(k_t) = \frac{1}{1-\alpha} k_t^{\alpha}.$$

Factor markets are competitive and factor rewards, respectively for capital and labor, correspond to

$$\rho_t = f'(k_t) = \frac{\alpha}{1-\alpha} k_t^{\alpha-1} \quad \text{and} \quad w_t = f(k_t) - k_t f'(k_t) = k_t^{\alpha}, \tag{1}$$

where ρ_t is decreasing and w_t is increasing in k_t.

Agents are born at the beginning of each period and stay active for two periods. Young agents are endowed with one unit of labor and work in their first period. At the end of their first period, i.e. at the point of time $t+1$, they earn the factor reward of labor, save everything and thus accumulate wealth. At the same point of time, the young generation becomes the old generation and they have to decide how to use their wealth (accumulated in the form of the numeraire and denoted by w_t) in order to maximize their consumption at the end of their second period.

Agents have three possibilities to allocate wealth: (1) they can invest in a Good project, (2) they can start a Bad investment project or (3) they can lend funds to other agents of the same generation. Investing in Good projects involves using the final good as capital input for the next period production, k_{t+1}. Assuming perfect foresight, the expected return of this investment project type is equal to the marginal product of capital, $\rho^e_{t+1} = \rho_{t+1}$. Thus, Good projects fuel production processes that generate labor income for the next generation. In contrast, Bad projects do not involve production processes. They can be seen as simple trading or storing activities, which fail to create any positive externalities for the next generations. Bad projects require an indivisible amount of m units of the final good and convert it into mB units of the final good in $t+1$, where $B > 0$ indicates the respective profitability. At this point, Matsuyama et al. (2016) introduce financial markets: By assumption, Bad projects require credit financing, thus $m > w_t$ holds. As a consequence, lending for Bad projects is a third option for wealth allocation. Given the possibility

of investing in Good projects, in equilibrium, the interest rate on credit has to be equal to the expected marginal product of capital $r_{t+1} = \rho^e_{t+1}$.

Credit markets are modeled as imperfect markets. Following the pledgeability approach proposed by Tirole (2005), it is assumed that agents can borrow only against collateral and that only a fraction of the expected project revenue, $0 < \mu_{t+1} < 1$ (in our framework, this fraction can vary through time; for this reason, differently from Matsuyama (2013) and Matsuyama et al. (2016), we call it henceforth *pledgeability ratio*), can be pledged for the repayment. Thus, the *borrowing constraint (BC)* requires that:

$$\mu_{t+1} mB \geq r_{t+1}(m - w_t) \qquad \text{or} \qquad \frac{\mu_{t+1} mB}{m - w_t} \geq r_{t+1}. \tag{2}$$

The lender will only lend up to $\frac{\mu_{t+1} mB}{r_{t+1}}$ which implicitly sets a minimum net worth requirement for agents interested in starting a Bad project. Thus, the net worth of the agents, w_t, is crucial for their position in the credit market. Matsuyama (2013) and Matsuyama et al. (2016) capture this financial friction with an exogenous pledgeability parameter summarizing all agency problems without any explicit reference to microeconomic or behavioral arguments.

Following a more behavioral approach, we endogenize the pledgeability ratio. In particular, we hypothesize that with a higher level of net worth the credit market sentiments may turn more optimistic. The risk perception is lower, which translates – in the context of our model – into a higher pledgeability ratio. With a lower level of net worth, the opposite holds. We thus assume that the pledgeability ratio positively depends on the level of net worth. Given the significant empirical evidence that credit market processes are highly non linear and discontinuous,[7] we do not specify a continuous relationship, but we allow for a dynamic regime switching between an optimistic and a pessimistic regime. Since we consider credit market sentiments to be determined by agents' net worth, we specify a related threshold, $\overline{w}$, expressing the overall business mood of lenders that may impact on their attitude towards risk. For $w_t > \overline{w}$ agents take an optimistic view concerning the ability of borrowers to return their debt; vice versa for $w_t < \overline{w}$ they take a pessimistic view. A high $\overline{w}$ indicates that agents are reluctant to switch to the optimistic regime (i.e. they only switch at a high overall net worth), which may correspond to a more risk-averse attitude. A low $\overline{w}$ suggests that agents may switch easily to the optimistic regime (i.e. they switch at a low overall net worth), corresponding to a less risk-averse attitude.

Incorporating these ideas, we specify the following law of motion for the pledgeability ratio:

$$\mu_{t+1} = \begin{cases} (1-\zeta)\mu_t + \zeta\mu_P & \text{if } w_t \leq \bar{w} \\ (1-\zeta)\mu_t + \zeta\mu_O & \text{if } w_t \geq \bar{w} \end{cases} \tag{3}$$

The pledgeability ratio itself, μ_{t+1}, follows a mean-reverting process: it is given as a weighted average, $\zeta \in [0, 1]$ between its current value μ_t and a long-run value μ_i with $i \in O, P$. We assume $\mu_O > \mu_P$, since in an optimistic regime the risk perception is lower and agents are ready to accept a higher fraction of the return on a Bad project as collateral. With a high ζ, a regime switch leads to an abrupt change in the pledgeability ratio; whereas a low ζ indicates a more sluggish adjustment after a regime switch.[8]

Moreover, the agents' choice of investment does not only depend on the access to credit (borrowing constraint), but also on their considerations about profitability. Agents only intend to start Bad projects, if the respective return is greater or equal to the return of simple lending or investing in Good projects. Thus, a *profitability constraint (PC)* requires

$$B \geq r_{t+1} = \rho^e_{t+1} (= f'(k_{t+1})) = \rho_{t+1}, \tag{4}$$

and sets a tighter limit than the borrowing constraint (equation (2)), if

$$\frac{\mu_{t+1} mB}{m - w_t} > B \qquad \text{or} \qquad w_t > m(1 - \mu_{t+1}). \tag{5}$$

[7] Brunnermeier and Sannikov (2014), for example, report high nonlinearity in amplification effects on credit markets. In empirical macroeconomic models, such non-linearities are quite often modeled as dynamic processes that involve two or more regimes, which are separated by thresholds (Mendoza and Terrones 2008, De Luigi and Huber 2018, Huber and Zörner 2019).

[8] One may consider the weighting parameter also to depend on the prevailing credit market sentiment. For the sake of parsimony, we omit this consideration in the paper and leave it for further research.

Analogously to Matsuyama et al. (2016), we define the maximal pledgeable rate of return, $R(w_t, \mu_{t+1})$, that an agent with the net worth w_t can pledge to the lender without violating a constraint:

$$R(w_t, \mu_{t+1}) \equiv B \min\Big\{\frac{\mu_{t+1}}{1 - w_t/m}, 1\Big\} = \begin{cases} \dfrac{\mu_{t+1} B}{1 - \frac{w_t}{m}} & \text{if } w_t \leq m(1-\mu_{t+1}) \quad \text{i.e. if BC is tighter} \\ B & \text{if } w_t \geq m(1-\mu_{t+1}) \quad \text{i.e. if PC is tighter.} \end{cases} \tag{6}$$

Note, that compared to the benchmark model, the perception of the financial friction is now endogenously determined by equation (3). After crossing the critical net worth threshold $w_t \geq m(1-\mu_{t+1})$ agents can pledge their full expected return B to the lender and thus no longer have borrowing constraints. This completes the model description.

We would like to point out that our modeling of the agents' behavior is based upon homogeneous agents – the whole continuum of agents switches simultaneously between the regimes and entertain the same risk perception and thus the same pledgeability ratio. In contrast, many models analyzing behavior on financial markets involve heterogeneous agents that have group specific behavioral patterns and may exhibit the phenomenon of herding.[9] With homogeneous agents the full unit measure of agents is either optimistic or pessimistic – the whole collective switches beliefs such that herding is not an issue. The study of López-Salido et al. (2017) on behavioral aspects supports our choice. In addition, as mentioned in Matsuyama (2008), homogeneous agents can be seen as a limiting case for heterogeneous agents switching slowly between the regimes.[10]

3 The dynamic equations

We are now ready to derive the law of motion for the net worth. In equilibrium, the following relation must hold with equality:

$$\rho^e_{t+1} = \rho_{t+1} = r_{t+1} = f'(k_{t+1}) \geq R(w_t, \mu_t).$$

If $\rho_{t+1} = r_{t+1} < R(w_t, \mu_t)$, agents would always prefer Bad projects (because of the potential higher returns), but nobody would provide the required credit as the rate of return of lending is too low, which is a contradiction and therefore not possible. In the case of $\rho_{t+1} > R(w_t, \mu_t)$ agents would never run Bad projects due to a violation of the profitability or the borrowing constraint.

In their fully-fledged analysis, Matsuyama et al. (2016) differentiate a *distortionary* and a *non-distortionary* case.[11] We focus on the *distortionary case* where the borrowing constraint impinges upon the dynamics and financial frictions play an essential role.

Before specifying the dynamic system, we would like to provide some intuition of the dynamic processes involved. Starting from the observation of (w_t, μ_t), agents update their pledgeability ratio according to equation (3) resulting in a new value for μ_{t+1}. They also decide upon their investment strategy, depending on (w_t, μ_{t+1}). For a low net worth, w_t, agents do not start Bad projects because of the higher profitability of Good projects. With a higher w_t the profitability of Good projects becomes lower; eventually the profitability of both investment types will be equal and the agents start strictly preferring Bad projects. However, since the wage rate and thus the net worth are still low, the maximum pledgeable rate of return for credit is lower than the return on Good investments. Agents cannot obtain the required credit. The borrowing constraint is still binding and agents continue to invest only in the Good projects, which results in the following law of motion:

$$w_{t+1} = w_t^{\alpha}. \tag{7}$$

[9] For example, Day and Huang (1990) introduce fundamentalists, chartists and herding into financial market modelling. Agents switch between groups depending upon the success of the respective behavioral rule according to an evolutionary selection dynamic. In addition, many macroeconomic models use different rules for expectation formation with a possibility of switching (Hommes, 2006; Chiarella et al., 2015; De Grauwe and Macciarelli, 2015). Typically, these models do not involve discontinuities. However, in some models, the behavioral rules involve a change in behavior once a threshold is crossed (Tramontana et al., 2013; Schmitt et al., 2017).

[10] However, one can easily model different group sizes of optimistic and pessimistic agents but needs to take into account that the dynamics involved will be much more complicated.

[11] In the *non-distortionary* case agents are never borrowing constrained. Therefore, the borrowing constraint is never binding in the equilibrium and the financial friction does not affect the dynamics of the credit allocation. As we are interested in the role of different perceptions of the agency problems altering financial frictions, we do not discuss this case.

Higher values of w_t increase the maximum pledgeable rate of return on credit and ease the borrowing constraint. At a threshold w_c the borrowing constraint is satisfied with equality (while the entire net worth is still invested in Good projects, i.e. $k_{t+1} = w_t$) and the maximum pledgeable rate of return on credit is equal to the profitability of Good projects. This threshold is implicitly defined by $f'(k_{t+1})|_{k_{t+1}=w_t} = R(w_t, \mu_{t+1})$, or by

$$w_c = \left(\frac{1}{\mu_{t+1} B} \frac{\alpha}{1-\alpha} \left(1 - \frac{w_c}{m} \right) \right)^{\frac{1}{1-\alpha}}, \tag{8}$$

where μ_{t+1} is given in eq.(3).

Beyond this threshold, for $w_t > w_c$ credit starts to flow into Bad projects. Investment in the Good projects is determined by $f'(k_{t+1}) = R(w_t, \mu_{t+1})$. Solving for k_{t+1} and using $w_t = k_t^\alpha$, the law of motion is now given by

$$w_{t+1} = \left(\frac{1}{\mu_{t+1} B} \frac{\alpha}{1-\alpha} \left(1 - \frac{w_t}{m} \right) \right)^{\frac{\alpha}{1-\alpha}}, \tag{9}$$

where μ_{t+1} is given in eq.(3).

After crossing another threshold, which depends on μ_{t+1} given in eq.(3),

$$w_\mu = m \left(1 - \mu_{t+1} \right), \tag{10}$$

the borrowing constraint is not binding anymore and investment in Good projects, k_{t+1}, is determined by the profitability constraint, i.e. by $f'(k_{t+1}) = B$. All additional credit flows into Bad projects and the dynamics follow

$$w_{t+1} = \left(\frac{\alpha}{B(1-\alpha)} \right)^{\frac{\alpha}{1-\alpha}}. \tag{11}$$

Thus, the dynamics of the *distortionary* case, extended with variable credit market sentiments affecting financial frictions, can be summarized by a two-dimensional piecewise smooth map that is discontinuous for $\overline{w}$ and $\zeta < 1$:

$$(w_{t+1}, \mu_{t+1}) = T(w_t, \mu_t) = \begin{cases} T_L(w_t, \mu_t) & if \quad w_t < \overline{w} \\ T_R(w_t, \mu_t) & if \quad w_t > \overline{w} \end{cases} \tag{12}$$

$$T_L(w_t, \mu_t) : \begin{cases} w^L_{t+1} = \begin{cases} w_t^\alpha & if \quad w_t \le w_c^L \\ \Psi^L_M(w_t, \mu_t) & if \quad w_c^L \le w_t \le w_\mu^L \\ \widehat{\beta} & if \quad w_t \ge w_\mu^L \end{cases} \\ \mu^L_{t+1} = (1-\zeta)\mu_t + \zeta \mu_P \end{cases} \tag{13}$$

$$T_R(w_t, \mu_t) : \begin{cases} w^R_{t+1} = \begin{cases} w_t^\alpha & if \quad w_t \le w_c^R \\ \Psi^R_M(w_t, \mu_t) & if \quad w_c^R \le w_t \le w_\mu^R \\ \widehat{\beta} & if \quad w_t \ge w_\mu^R \end{cases} \\ \mu^R_{t+1} = (1-\zeta)\mu_t + \zeta \mu_O \end{cases} \tag{14}$$

$$\Psi^L_M(w_t, \mu_t) = \left(\frac{m - w_t}{m\beta((1-\zeta)\mu_t + \zeta\mu_P)} \right)^{\frac{\alpha}{1-\alpha}}, \quad \Psi^R_M(w_t, \mu_t) = \left(\frac{m - w_t}{m\beta((1-\zeta)\mu_t + \zeta\mu_O)} \right)^{\frac{\alpha}{1-\alpha}} \tag{15}$$

where $\beta = B^{\frac{1-\alpha}{\alpha}}$ and $\widehat{\beta} = \left(\frac{1}{\beta} \right)^{\frac{\alpha}{1-\alpha}}$, w_c^L and w_c^R are defined in equation (8), and μ_{t+1} is given as in $T_L(w_t, \mu_t)$ an $T_R(w_t, \mu_t)$, resp. Finally,

$$w_\mu^L = m(1 - ((1-\zeta)\mu_t + \zeta\mu_P)) \quad \text{and} \quad w_\mu^R = m(1 - ((1-\zeta)\mu_t + \zeta\mu_O)), \tag{16}$$

see also equation (10), where the respective values for μ_{t+1} are used.

On the discontinuity line $w_t = \overline{w}$ we have $T_L(\overline{w}, \mu_t) = (w^L_{t+1}, (1-\zeta)\mu_t + \zeta\mu_P)$ and $T_R(\overline{w}, \mu_t) = (w^R_{t+1}, (1-\zeta)\mu_t + \zeta\mu_O)$ so that the pledgeability ratio, μ_{t+1}, has a jump corresponding to $\mu^R_{t+1} - \mu^L_{t+1} = \zeta(\mu_O - \mu_P)$.

The system thus has seven parameters, $\alpha, m, B, \mu_P, \mu_O, \overline{w}$ and ζ, where the following restrictions apply: $0 < \alpha, \mu_P, \mu_O, \overline{w}, \zeta < 1$, $\mu_O > \mu_P$, $m > 1$ and $B > 0$. Note that for $\overline{w} = 1$ and $\zeta = 1$ the model reduces

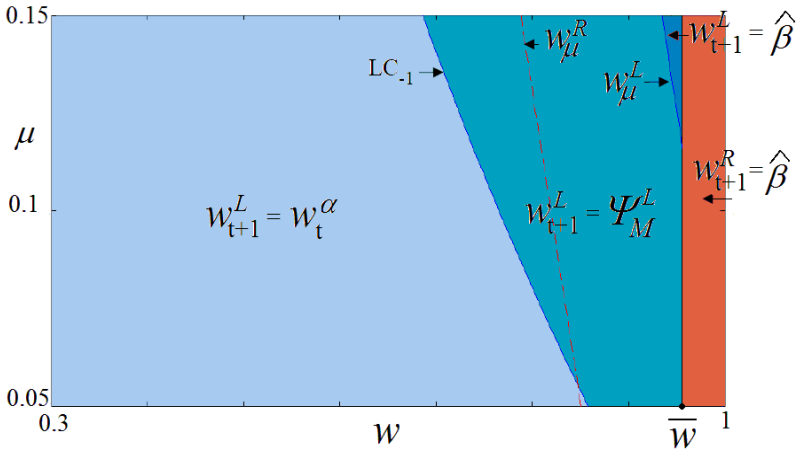

Figure 1: Phase plane (w, μ) for $\overline{w} = 0.955$, $\mu_O = 0.4$ and $\zeta = 0.4$. These parameters are used in some examples in the next section and in Appendix.

to the benchmark model. Due to the normalization, $(1-\alpha)A = 1$ the system is restricted on $(0, 1]$. Some parameters are fixed throughout the whole paper as follows:

$$\alpha = 0.33,\ m = 1.05,\ B = 2,\ \mu_P = 0.05, \tag{17}$$

and thus are not reported in the figure captions. Fig.1 represents the phase space at parameter values which will be used in some numerical simulations and commented in the next section. The discontinuity line $w = \overline{w}$ separates the plane in two partitions, denoted by L $(w < \overline{w})$, where the function T_L applies (evidenced in blue), and R $(w > \overline{w})$, where the function T_R applies (evidenced in red). The critical line LC_{-1} is the locus of points w_c^L implicitly defined by $\left(w_c^L\right)^\alpha = \Psi_M^L(w_c^L, \mu)$ for any $\mu \in (0, 1]$ and separates the two regions in which the function T_L has different smooth definitions. One more region is evidenced in dark blue in the L partition, bounded by the line w_μ^L (see eq.(16)), where the function T_L is defined by the constant value $\widehat{\beta}$. On the right side of $\overline{w}$, in the example considered in Fig.1, the function T_R is defined by the constant value $\widehat{\beta}$, since the region belongs to the right side of the line w_μ^R (see eq.(16)).

The fixed points of map T are given by

$$(w^{*L}, \mu_P) \text{ if } w^{*L} < \overline{w}\ ,\quad (w^{*R}, \mu_O) \text{ if } w^{*R} > \overline{w} \tag{18}$$

Assuming $w \in (0, 1)$ the monotone increasing branch w^α has no fixed point; if $\widehat{\beta} \geq m(1-\mu_P)$ then $w^{*L} = \widehat{\beta}$; if $\widehat{\beta} < m(1-\mu_P)$, w^{*L} is the solution of $w^{*L} = \left(\frac{m-w^{*L}}{m\beta\mu_P}\right)^{\frac{\alpha}{1-\alpha}}$ which may lead to an actual fixed point (if $w^{*L} < \overline{w}$) or a virtual one,[12] otherwise. Similarly in the R side: if $\widehat{\beta} \geq m(1-\mu_O)$ then $w^{*R} = \widehat{\beta}$; if $\widehat{\beta} < m(1-\mu_O)$, w^{*R} is the solution of $w^{*R} = \left(\frac{m-w^{*R}}{m\beta\mu_O}\right)^{\frac{\alpha}{1-\alpha}}$ which may lead to an actual fixed point or a virtual one.

Notice that for a fixed value for $\overline{w}$ the functions T_L and T_R are of triangular structure, that is, one component (μ_{t+1}) is independent of the other (w_{t+1}). Thus, the Jacobian matrix is also triangular, with eigenvalues on the diagonal, and eigenvectors parallel to the coordinate axes. For T_L we have

$$J_{T_L}(w_t, \mu_t) = \begin{bmatrix} \frac{\partial}{\partial w_t}\Psi_M^L & \frac{\partial}{\partial \mu_t}\Psi_M^L \\ 0 & (1-\zeta) \end{bmatrix} \tag{19}$$

with

$$\frac{\partial}{\partial w_t}\Psi_M^L(w_t, \mu_t) = \frac{-\alpha}{1-\alpha}\left(\frac{m-w_t}{m\beta((1-\zeta)\mu_t + \zeta\mu_P)}\right)^{\frac{\alpha}{1-\alpha}}\frac{1}{m-w_t}. \tag{20}$$

[12] A fixed point is called real if it belongs to the related region of definition of the function (T_L or T_R), otherwise it is called virtual (for example if the fixed point of the function T_L belongs to the right partition, then it is virtual, and thus it is not a fixed point of map T).

Evaluating at the fixed point (w^{*L}, μ_P) and using $\left(\frac{m-w^{*L}}{m\beta\mu_P}\right)^{\frac{\alpha}{1-\alpha}} = w^{*L}$ it follows that the eigenvalues are given by:

$$\lambda_1 = -\frac{\alpha}{1-\alpha}\frac{w^{*L}}{m-w^{*L}} \quad , \quad \lambda_2 = 1-\zeta \in (0,1). \tag{21}$$

The (local) eigenvector related to λ_2 is on the line $\mu = \mu_P$ and the (local) eigenvector related to λ_1 is on the line $w = w^{*L}$. Since $\lambda_2 \in (0,1)$, the fixed point may have a flip bifurcation when the eigenvalue λ_1 crosses the value -1. Thus, w^{*L} is stable for

$$\lambda_1 = -\frac{\alpha}{1-\alpha}\frac{w^{*L}}{m-w^{*L}} > -1 \text{ iff } w^{*L} < m(1-\alpha). \tag{22}$$

Similarly for T_R, when evaluated at the fixed point (w^{*R}, μ_O), the eigenvalues are given by:

$$\lambda_1 = -\frac{\alpha}{1-\alpha}\frac{w^{*R}}{m-w^{*R}}, \quad \lambda_2 = 1-\zeta \in (0,1). \tag{23}$$

The (local) eigenvector related to λ_2 is on the line $\mu = \mu_O$ and the (local) eigenvector related to λ_1 is on the line $w = w^{*R}$, and w^{*R} is stable for

$$\lambda_1 = -\frac{\alpha}{1-\alpha}\frac{w^{*R}}{m-w^{*R}} > -1 \text{ iff } w^{*R} < m(1-\alpha). \tag{24}$$

Note that the value of these fixed points (and related stability conditions) are independent of the parameters ζ and $\overline{w}$. However, as seen above, $\overline{w}$ can determine their existence (i.e. if one, two or none of them exists). That is, a fixed point may not only lose stability via a flip bifurcation but it may "appear/disappear" by border collision,[13] colliding with $\overline{w}$. This border collision bifurcation (BCB for short) occurs when $w^{*L} = \overline{w}$ or $w^{*R} = \overline{w}$. It follows that for $w^{*L} < \overline{w} < w^{*R}$ both fixed points exist; or only one of them exists: (w^{*L}, μ_P) if $w^{*L} < \overline{w}$, (w^{*R}, μ_O) if $w^{*R} > \overline{w}$; or no fixed point exists for $w^{*R} < \overline{w} < w^{*L}$ (both are virtual).

4 Behavioral parameters and their dynamic implications

Our model comprises the following behavioral dimensions:

- Agents are considered to switch between an optimistic and a pessimistic credit market sentiment, depending upon $w \lessgtr \overline{w}$, the higher $\overline{w}$, the less likely the optimistic regime $w > \overline{w}$ will occur.
- Credit market sentiments impact upon the fundamental perception of agency problems, reflected in μ_O and μ_P.
- Finally, agents are assumed to behave sluggishly when revising their perception of the agency problems, reflected in the adjustment parameter ζ.

We are in particular interested how in these behavioral dimensions interact with the dynamic mechanism presented in Matsuyama (2016) and how they impact upon macroeconomic stability. Therefore, in all our simulations we consider fixed the parameters as given in (17) at which the Matsuyama's model exhibits chaotic fluctuations, and investigate whether the behavioral dimensions have a stabilizing influence on the dynamics.

In order to structure our analysis, we choose the following strategy: As case 1, we analyze a situation in which the fundamental perceptions of the agency problems differ substantially between an optimistic and a pessimistic credit market sentiment. In case 2, the difference between μ_O and μ_P is much smaller. In both cases, we investigate the effects of varying $\overline{w}$ and ζ.

[13] In piecewise smooth maps, a "border collision" occurs whenever an invariant set (typically a periodic point of a cycle, but not only) collides with the set at which the definition of the map changes.

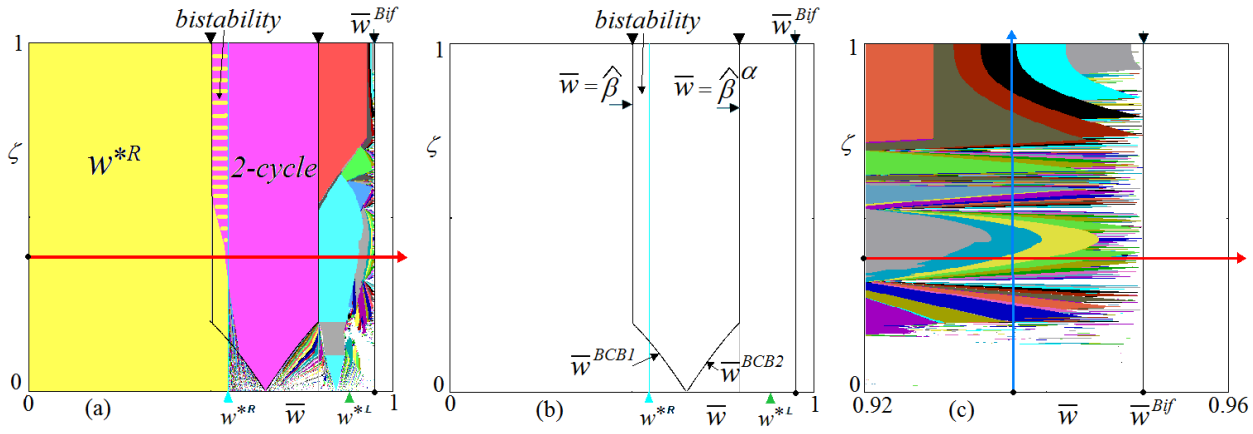

Figure 2: In (a) two-dimensional bifurcation diagram in the parameter plane $(\overline{w}, \zeta)$ for $\mu_O = 0.4$. The colors are related to the period of the cycles. The white region denotes either cycles of period larger than 45 or chaotic dynamics. In (b) only some bifurcation curves are shown, and $\overline{w}^{Bif} = 0.95059$. In (c) an enlargement of (a). The arrows denote parameter paths for the one-dimensional bifurcation diagrams shown in Fig.3 and Fig.4, the red line is drawn at $\zeta = 0.4$, the blue vertical line at $\overline{w} = 0.935$.

4.1 Case 1: Strong effect upon the pledgeability ratio

In the case considered in this subsection, the change to an optimistic credit market sentiment has a strong impact upon the fundamental value of the pledgeability ratio. Thus, we assume a comparatively high value of μ_O, $\mu_O = 0.4$. In Fig.2 we represent a two dimensional bifurcation diagram, in which $\overline{w}$ and ζ are varied between 0 and 1. The bifurcation curves shown in Fig.2(b) are explained below.

The benchmark of Matsuyama (2016) is represented by the top right corner $(\overline{w}, \zeta) = (1, 1)$ and, as already noticed, it exhibits chaotic dynamics for the chosen parameters (given in (17)). At first glance, introducing behavioral components appears to stabilize the dynamics, leading to cycles with low periodicity and even to fixed points. This is particularly evident when lowering $\overline{w}$; i.e. allowing for an easier switch to an optimistic credit market sentiment. Surprisingly, this is less evident when lowering ζ; i.e. when introducing a more persistent behavior. In the following, we provide a detailed analysis of the dynamics.

The fixed points of the map are given by $\left(w^{*R}, \mu_O\right) = (0.5475, 0.4)$ and $\left(w^{*L}, \mu_P\right) = (0.8825, 0.05)$. For $\overline{w} < w^{*R}$ (the value w^{*R} is marked by an azure arrow in Fig.2(a,b)), the fixed point in the R partition exists and is attracting (yellow area). For $\overline{w} > w^{*L}$ (the value w^{*L} is marked by a green arrow in Fig.2a) the fixed point in the L partition exists, but it is a saddle; apparently, its disappearance at $\overline{w} = w^{*L} = 0.8825$ (decreasing $\overline{w}$) does not affect the existing attracting cycles (that is, no change is observed in the attracting set of the map).

The pink area in Fig.2(a) indicates the existence of an attracting 2-cycle. Due to the triangular structure of the map, an (almost) complete analytic description of the corresponding bifurcations is possible (see Appendix 7.1 for details). The points of the 2-cycle whose existence region is evidenced in Fig.2a, denoted by (w_R, μ_R) and (w_L, μ_L), belong to the right and left partition, respectively, satisfy $T_L(w_L, \mu_L) = (w_R, \mu_R)$ and $T_R(w_R, \mu_R) = (w_L, \mu_L)$, so that μ_R and μ_L can easily be obtained explicitly:

$$\mu_R = \mu_O - \frac{\mu_O - \mu_P}{2 - \zeta} \quad \text{and} \quad \mu_L = \mu_P + \frac{\mu_O - \mu_P}{2 - \zeta}. \tag{25}$$

In the case shown in Fig.2a, for high values of ζ, the first component of the two periodic points is given by $w_L = \widehat{\beta}$ and $w_R = (\widehat{\beta})^{\alpha}$. The related BCBs occur when a periodic point merges with $\overline{w}$, that is, for $\overline{w} = \widehat{\beta}$ and $\overline{w} = (\widehat{\beta})^{\alpha}$, respectively, where $\widehat{\beta} < (\widehat{\beta})^{\alpha}$, see the vertical black lines in Fig.2(a,b). For lower values of ζ, a different kind of 2-cycle exists, involving the periodic points $w_R = \Psi_M^L(w_L, \mu_L)$ and $w_L = \Psi_M^R(w_R, \mu_R)$. We do not have an explicit solution for the BCBs of these two periodic points, that occur at the collision with $\overline{w}$, thus the bifurcation curves in Fig.2(a,b) denoted as $\overline{w}^{BCB1}$ (when $w_L = \overline{w}$) and $\overline{w}^{BCB2}$ (when $w_R = \overline{w}$) are detected only numerically.

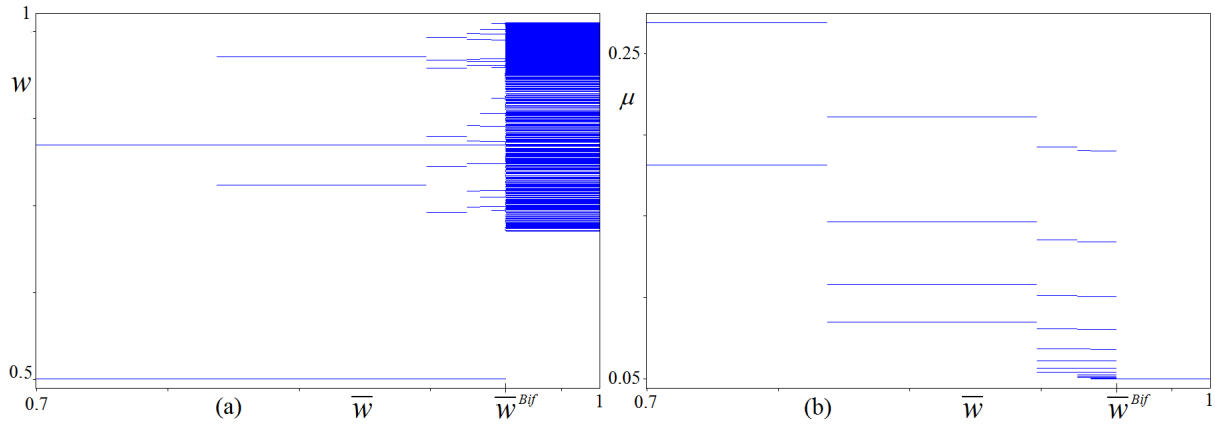

Figure 3: One-dimensional bifurcation diagrams as a function of $\overline{w}$ for $\mu_O = 0.08$ and $\zeta = 0.4$. Panel (a) shows the dynamics of w, and panel (b) the dynamics of μ. In both panels, $\overline{w}^{Bif} = 0.95059$.

From Fig.2(a) we have evidence that the existence regions of a stable fixed point and a stable 2-cycle are overlapping, so we have regions of coexistence. This phenomenon of coexisting attractors has important economic implications. A sudden change in the initial conditions, e.g. in the agent's net worth w_t, but also to the pledgeability ratio μ_t, may change the system's long-run outcome from a stable fixed point to a 2-cycle. The coexistence of attractors may prevent the restoration of the original dynamic pattern. Thus, there is no correction back to the initial situation and exogenous and transitory shocks have the potential to change the cyclical properties in the long run and thus to have persistent effects. This is of particular interest in our model framework, which is designed to incorporate systematic components in behavioral financial decisions (involving $\overline{w}$, μ_O and μ_P, and ζ). Nevertheless, given the volatility of financial markets, other influences on μ_t cannot be excluded; in our model, these can be treated as exogenous shocks. Given the coexistence of attractors, the shocks – even if only transitory – have the potential to persistently change the long-run cyclical behavior (by moving the dynamics from one attractor to the other). As already remarked above, the coexistence of attractors introduces also an element of hysteresis; a shock of equal size, but in the opposite direction, will not necessarily restore the original situation.

We now study in more detail the role of variations of the business mood, operationalized by changes of the behavioral threshold $\overline{w}$. For $\overline{w} = 1$, the market is always in the pessimistic state, i.e. $\mu_t = \mu_P$. Lowering $\overline{w}$ opens the possibility that the credit market sentiment changes to an optimistic state, the lower $\overline{w}$, the easier this switch occurs. Thus, lowering $\overline{w}$ introduces regime switching as an additional dynamic process. Fig.3 represents a one dimensional bifurcation diagram on $\overline{w}$, drawn for $\zeta = 0.4$; it corresponds to the red arrow in Fig.2(a,c).

Fig.3(a) shows the dynamics of the net worth w_t. It reveals a stabilizing effect of a reduction in $\overline{w}$, because the transition is from chaotic motion of w_t, to cycles with a high periodicity, to cycles with a low periodicity and finally to a fixed point. Fig.3(b) shows the corresponding dynamics in the pledgeability ratio μ_t. It exhibits further remarkable properties: the chaotic dynamics for w_t, which appears for high values of $\overline{w}$, actually involves a constant $\mu = \mu_P = 0.05$; thus, the corresponding attractor is one-dimensional and corresponds to a chaotic interval.

The reason is the following. As mentioned above, the fixed point $\left(w^{*L}, \mu_P\right) = (0.8825, 0.05)$ exists for $\overline{w} > w^{*L}$, but it is a saddle. Thus, for $\overline{w} = 1$ the two-dimensional map has a vertical eigenvector, related to the eigenvalue smaller than 1, which attracts trajectories to the line $\mu = \mu_P$. The asymptotic dynamics - for $\overline{w} = 1$ and $0 < \zeta \leq 1$ - occur at a constant value of μ, $\mu = \mu_P$, and the system reduces to a one-dimensional map, whose shape is similar to that of the Matsuyama (2016) map. For the chosen parameters (given in (17)), the benchmark map is in a chaotic regime, for which the attracting set is a chaotic interval $I = [C_1, C]$. It is bounded by two critical points, C and C_1, which are the iterates of the critical point C_{-1} (which is the point of local mximum, and it corresponds to the intersection of the critical line LC_{-1} shown in Fig.1 with the line $\mu = \mu_P$). Decreasing $\overline{w}$, the one-dimensional attracting set continues to exist. Its structure changes, becoming a two-dimensional attracting set, at the BCB bifurcation occurring when $C = \overline{w}$. As shown in

Appendix 7.2, this bifurcation occurs at $\overline{w}^{Bif} = (\widetilde{w})^{\alpha}$, where $\widetilde{w}$ is implicitly given by

$$\left(\frac{m-\widetilde{w}}{m\beta\mu_P}\right)^{\frac{1}{1-\alpha}} = \widetilde{w}. \tag{26}$$

This bifurcation involves the transition from an attracting set only on the L partition of the map and on the line $\mu = \mu_P$ (a chaotic interval) to an attracting set of the plane, involving the right partition of the map, where the function T_R applies and it is defined by the constant value $\widehat{\beta}$. This leads to an attracting set which is in general a superstable cycle[14] which includes the periodic point $\left(\widehat{\beta}, \widehat{\mu}\right)$, where

$$\widehat{\mu} = (1-\zeta)\mu_P + \zeta\mu_O, \tag{27}$$

and involving switches between an optimistic and a pessimistic credit market sentiment (and thus involving cyclical values for the pledgeability ratio μ_t). As we can see from the implicit equation in (26), the bifurcation value $\overline{w}^{Bif}$ is independent of ζ and of μ_O (see the corresponding vertical line in Fig.2).

This analysis helps us to clarify the interplay between the behavioral regime switching and Matsuyama's mechanism generating endogenous cycles: At a high value of $\overline{w}$, agents are very reluctant to switch to another behavioral regime, actually on the attractor no such switch occurs. The dynamics (that is chaotic, for the chosen parameters) is driven entirely by Matsuyama's mechanism based on financial frictions. With a lower $\overline{w}$, regime switches occur and in optimistic phases agents increase their pledgeability ratio μ_t. Note that a higher pledgeability ratio μ_t actually reflects lower financial market imperfections – and the softening of financial frictions potentially stabilizes the dynamics (from chaotic to cyclical with lower and lower periodicity). However, Fig.3(a) reveals also an additional pattern in the dynamics where behavioral regime switching plays a relevant role: After the transition from chaotic to cyclical attractors, the cycles in net worth w_t involve wider fluctuations, which hit the lower boundary $w = \widehat{\beta}$. This is because, after the transition, the behavioral regime switch takes effect allowing for stronger reactions in net worth w_t (in comparison to those on the chaotic attractor) widening Matsuyama's endogenous credit cycles. In this sense introducing credit market sentiments has also a destabilizing effect on the economy and the first impression of a stabilizing effect of a reduction in $\overline{w}$ needs qualification. Note in addition that a reduction in $\overline{w}$ tends to reduce the average net worth over the cycle (see Fig.3(a)).

Finally, we discuss the role of sluggish adjustment of the pledgeability ratio, i.e. in the role of ζ, where a low value of ζ represents a more persistent behavior (less sharp swings in the pledgeability ratio). The one-dimensional bifurcation diagrams in Fig.4(a,b) show the effect of varying ζ. It is computed for $\overline{w} = 0.935 < \overline{w}^{Bif}$ ($\overline{w}^{Bif} = 0.95059$ for the chosen parameters) and corresponds to the vertical blue arrow in Fig.2(c). For high values of ζ the superstable cycles with a long periodicity involving $w = \widehat{\beta}$ are well visible. At a lower value of ζ, these cycles bifurcate into a chaotic attractor. In Appendix 7.3, we show that this bifurcation occurs at

$$\zeta^{Bif} = \frac{m\left(1-\mu_P\right) - \widetilde{w}^{\alpha}}{m\left(\mu_O - \mu_P\right)}. \tag{28}$$

At this threshold, evidenced in Fig.4(a), decreasing ζ a transition occurs from a two-dimensional attracting set, which is a superstable cycle including the point $\left(\widehat{\beta}, \widehat{\mu}\right)$, to a two-dimensional attracting set, which is chaotic (and such that $w_t > \widehat{\beta}$ for all t). Note that a lower value of μ_O increases this threshold value ζ^{Bif}. Note in addition that this transition – while involving an increase in complexity (cyclical vs chaotic attractor) – reduces the range of fluctuations of w_t (since, as commented above, the value $\widehat{\beta}$ is no longer reached).

This pattern is in line with economic intuition: A reduction in ζ reflects a more sluggish behavior, which implies that the effects of the regime switches are less pronounced. A lower value of μ_O (closer to μ_P) has a similar effect. Indeed, as noted in the previous section, at the discontinuity line the jump in the (current) pledgeability ratio μ_t corresponds to $\zeta(\mu_O - \mu_P)$, which also weakens the behavioral dynamic process. In both cases (lower ζ and lower value of μ_O) Matsuyama's endogenous cycles mechanism driven by financial frictions (which are chaotic for the chosen parameters) dominates the dynamics.

[14] In one-dimensional maps a cycle is called superstable, when its eigenvalue is equal to zero. In our two-dimensional map we call a cycle superstable, when one of its periodic points belongs to a partition in which the map is defined by $w_{t+1}^R = \widehat{\beta}$, constant. The cycle has one eigenvalue equal to zero and the other smaller than 1, so that it is always attracting.

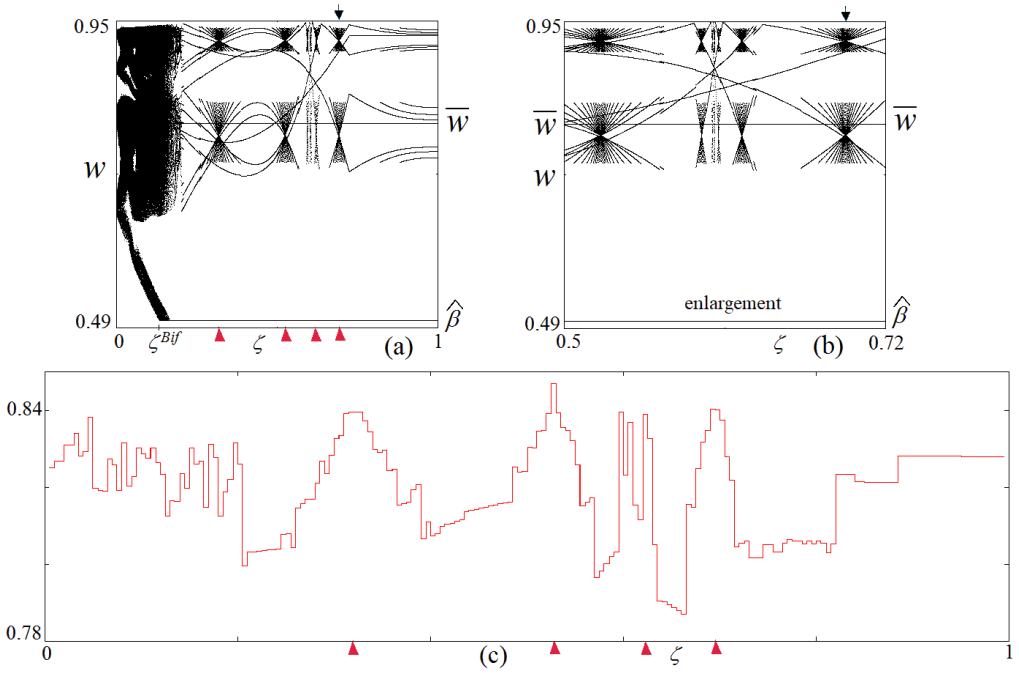

Figure 4: Panel (a) is a one-dimensional bifurcation diagram showing the dynamics of w as a function of ζ for $\overline{w} = 0.935$ and $\mu_O = 0.4$; in panel (a) and (b) $\zeta^{Bif} = 0.1276$. Panel (b) ia an enlargement of (a). Panel (c) shows the average of w over the cycles as a function of ζ. A few peaks in (a) and (c) are evidenced by red arrows.

We are now able to complete the description of Fig. 2(c) and to summarize the bifurcation structure: For the chosen parameters $\overline{w}^{Bif} = 0.95059$ and $\zeta^{Bif} = 0.1276$ hold. For $\overline{w}^{Bif} < \overline{w} < 1$ we observe a chaotic interval on the line $\mu = \mu_P$ for all values of ζ. Reducing $\overline{w}$ below $\overline{w}^{Bif}$, destroys the chaotic interval: For $\overline{w} < \overline{w}^{Bif}$ and $1 > \zeta > \zeta^{Bif} = 0.1276$ a superstable cycle appears involving the point $\left(\widehat{\beta}, \widehat{\mu}\right)$; for $\overline{w} < \overline{w}^{Bif}$ and $\zeta^{Bif} = 0.1276 > \zeta > 0$ a chaotic area appears (see Appendix 7.3).

In addition, Fig.4(a) and in particular the enlargement in Fig.4(b), reveals a particular structure of the superstable cycles described in Appendix 7.4. A reduction of ζ from the value 1 does not affect the range of the fluctuations in net worth w_t; however, it markedly changes its periodicity. As described in Appendix 7.4, all the cycles have the periodic point $(\widehat{\beta}, \widehat{\mu})$ and at first the periods of the cycles are reduced by 4 units. Then the periods start to increase by 4 at each subsequent bifurcation and we observe a kind of "spider structure"; at the center of the structure a Milnor attractor occurs,[15] marked by an arrow in Fig.4(a,b). Immeadiately after, the periods of the cycles start to decrease by 4 at each subsequent bifurcation. This kind of mechanism is repeated several times, as shown in Fig.4(a,b). This, actually, is a remarkable effect of lowering ζ , i.e. of increasing the behavioral inertia: For a wide range of ζ, it leads to a swing between phases with period reduction and with period increase, without significant changes in the range of variability of w_t. Note however, that periodic points added (and lost) involve comparatively high values of w_t (only one point of each cycle is located on the lower boundary); therefore, cycles with a higher periodicity exhibit a higher average net worth. Interestingly, reducing ζ thus leads to swings in the average net worth. Fig. 4(c) shows the average net worth and reveals that it peaks whenever the periodicity is high (i.e. close to the centers of each "spider structure"). Therefore, it seems that adding behavioral inertia adds complexity in a different dimension.

[15] A Milnor attractor is here a repelling cycle which attracts a set of points of positive Lebesgue measure.

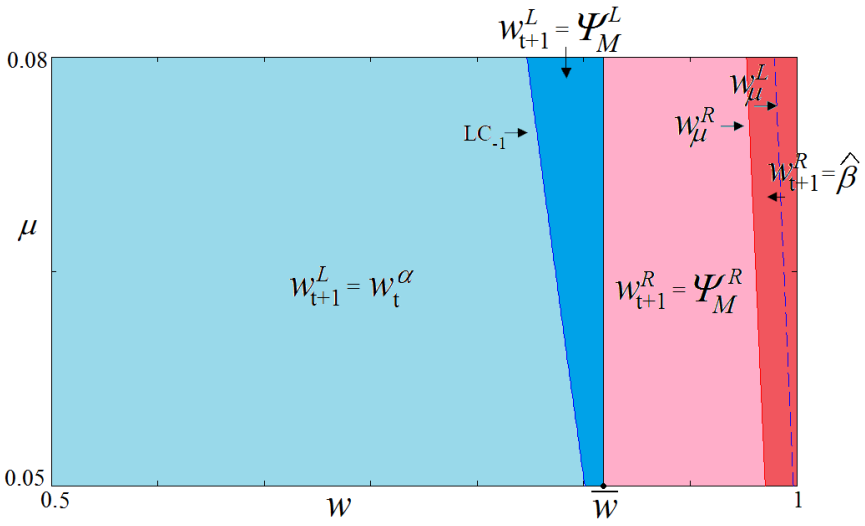

Figure 5: Phase plane (w, μ) for $\overline{w} = 0.8695$, $\mu_O = 0.08$ and $\zeta = 0.6$. These parameters are used in some examples below and in Appendix.

4.2 Case 2: Weak effect upon the pledgeability ratio

As case 2, we study a situation in which the change to an optimistic credit market sentiment has a weak impact on the fundamental value for the pledgeability ratio. We continue to use the parameters given in (17), for which the Matsuyama (2016) model exhibits chaotic fluctuations. However, we now assume a comparatively low value of μ_O, $\mu_O = 0.08$. The phase space is as depicted in Fig. 5. Note that this case is special, since $\overline{w} < w_c^L(\overline{\mu})$, where $\overline{\mu} = (1-\zeta)\mu_O + \zeta\mu_P$, is possible. Below we analyze this possibility in more detail; we stress here that it leads to a continuous one-dimensional map for $\zeta = 1$, which has an attracting 2-cycle on the line $\mu = \mu_O = 0.08$ (the fixed point in the right partition is a saddle, since it is $w^{*R} > m(1-\alpha) = 0.7035$, see in eq.(24)). For $\overline{w} < w_c^L(\overline{\mu})$ and $\zeta < 1$, $w_{t+1} = w_t^\alpha$ (which is independent of the pledgeability ratio) and the discontinuity only appears in the values of μ_t.

Fig.6 represents a two dimensional bifurcation diagram, in which ζ is varied between 0 and 1 and $\overline{w}$ between 0.5 and 1. We concentrate on the second half of the parameter space, $\overline{w} > 0.5$, because in the first half, for $\overline{w} \leq 0.5$, there always exists an attracting 2-cycle.

The bifurcation structure shows similarities to case 1: for any fixed value of ζ, decreasing $\overline{w}$ from the value 1, first a chaotic interval $[C_1, C]$ on the line $\mu = \mu_P = 0.05$ exists. Then, after the critical point C crosses the $\overline{w}$ threshold, the branch T_R of the map begins to play a role: if the border related to the flat branch on the right side is crossed $\left(w_\mu^R\right)$, then a superstable cycle occurs; otherwise, we have a chaotic attractor.

Similar to case 1, for lower values of $\overline{w}$ cycles with lower periodicity appear; again, an explicit bifurcation analysis is possible. Fig.6 evidences the existence of an attracting 3-cycle (red area in Fig.6(a)). It has the symbolic sequence LLR and thus its periodic points are defined by (w_1, μ_1), $(w_2, \mu_2) = T_L(w_1, \mu_1)$, $(w_3, \mu_3) = T_L(w_2, \mu_2)$, $(w_1, \mu_1) = T_R(w_3, \mu_3)$. In the case under consideration, $T_R(.)$ applies with Ψ_M^R while $T_L(.)$ applies with w^α. The values μ_i of the cycle can be determined explicitly (after some algebraic steps):

$$\begin{aligned} \mu_1 &= \mu_P + \frac{\mu_O - \mu_P}{\zeta^2 - 3\zeta + 3} \\ \mu_2 &= (1-\zeta)\mu_1 + \zeta\mu_P \\ \mu_3 &= (1-\zeta)^2\mu_1 + \zeta(2-\zeta)\mu_P. \end{aligned} \tag{29}$$

A BCB occurs when the condition $T_L^2 \circ T_R(\overline{w}, \mu_3) = (\overline{w}, \mu_3)$ is satisfied, leading to the condition $(\overline{w})^{\frac{1-\alpha}{\alpha^3}} =$

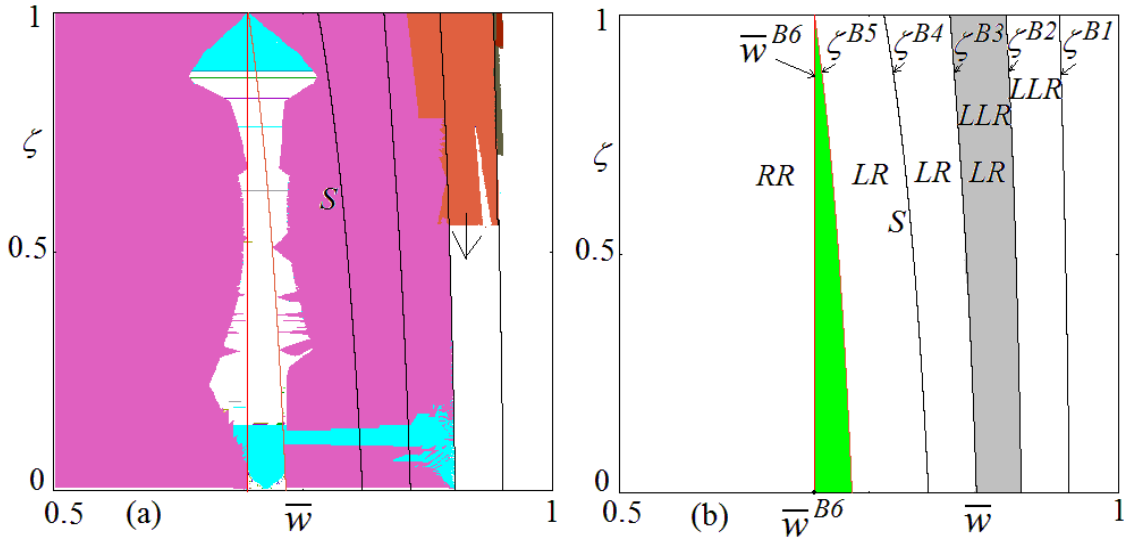

Figure 6: Panel (a) shows a two-dimensional bifurcation diagram in the parameter plane $(\overline{w},\zeta)$ for $\mu_O = 0.08$. Different colors denote different periods of the cycles. The pink area denotes an attracting 2-cycle. The white region denotes either cycles of period larger than 45 or chaotic dynamics. Panel (b) shows the bifurcation curves mentioned in the text. In panle (b), $\overline{w}^{B6} = 0.695$.

$\frac{m-\overline{w}}{m\beta[\mu_P+\frac{\mu_O-\mu_P}{\zeta^2-3\zeta+3}]}$, which can be solved for ζ obtaining

$$\zeta^{B1} = \frac{3}{2} - \frac{1}{2}\sqrt{\frac{(\mu_P - 4\mu_O)\, m\beta\,(\overline{w})^{\frac{1-\alpha}{\alpha^3}} + 3\,(m-\overline{w})}{\mu_P m\beta\,(\overline{w})^{\frac{1-\alpha}{\alpha^3}} - (m-\overline{w})}}, \tag{30}$$

which is the first bifurcation curve from the right side, shown in Fig.6. Fig.6(a) reveals that the 3-cycle loses stability for lower values of ζ (at the transition from the red region of the stable 3-cycle to the white region below it, marked by an arrow). This transition corresponds to a border collision of the attracting 3-cycle with a point of the critical line LC_{-1} of the map, after which the 3-cycle continues to exist but as a saddle (Appendix 7.5 illustrates this argument).

As we can see from Fig.6(a), continuing to decrease $\overline{w}$ a 2-cycle also appears. It has symbolic sequence LR so that its points satisfy $T_L(w_L,\mu_L) = (w_R,\mu_R)$ and $T_R(w_R,\mu_R) = (w_L,\mu_L)$, where μ_R and μ_L are explicitly given in eq.(25). A bifurcation occurs when the condition $T_L \circ T_R(\overline{w},\mu_R) = (\overline{w},\mu_R)$ holds, where $T_R(.)$ applies with Ψ_M^R while $T_L(.)$ applies with w^α, i.e. when $(\overline{w})^{\frac{1-\alpha}{\alpha^2}} = \frac{m-\overline{w}}{m\beta[\mu_P+\frac{\mu_O-\mu_P}{2-\zeta}]}$ is satisfied. Solving for ζ it leads to

$$\zeta^{B2} = 2 - \frac{\mu_O-\mu_P}{\frac{m-\overline{w}}{m\beta(\overline{w})^{\frac{1-\alpha}{\alpha^2}}} - \mu_P}, \tag{31}$$

which is the second bifurcation curve from the right side in Fig.6.

Decreasing $\overline{w}$ (at a fixed value for ζ), the attracting 3-cycle with symbolic sequence LLR disappears when the condition $T_L \circ T_R \circ T_L(\overline{w},\mu_2) = (\overline{w},\mu_2)$ occurs (where $T_R(.)$ applies with Ψ_M^R while $T_L(.)$ applies with w^α), i.e. when $(\overline{w})^{\frac{1-\alpha}{\alpha^2}} = \frac{m-(\overline{w})^\alpha}{m\beta[\mu_P+\frac{\mu_O-\mu_P}{\zeta^2-3\zeta+3}]}$ is satisfied. Solving for ζ it leads to

$$\zeta^{B3} = \frac{3}{2} - \frac{1}{2}\sqrt{4(\frac{\mu_O-\mu_P}{\frac{m-(\overline{w})^\alpha}{m\beta(\overline{w})^{\frac{1-\alpha}{\alpha^2}}} - \mu_P) - 3}, \tag{32}$$

which is the third bifurcation curve from the right side in Fig.6. Thus in the grey strip evidenced in Fig.6(b) we have coexistence of a 2-cycle and a 3-cycle.

Further decreasing $\overline{w}$, the structure of the map changes when the border point $\overline{w}$ crosses the critical point w_c, associated with the critial curve LC_{-1}, this occurs when the curve LC_{-1}, the line $w = \overline{w}$ and the line $\mu = \widehat{\mu}$ (where $\widehat{\mu}$ is explicitly given in eq.(27)) are intersecting in $(\overline{w}, \widehat{\mu})$, leading to the condition $\overline{w} = w_c$ and $\overline{w}^{\alpha} = \Psi_M^R(\overline{w}, \widehat{\mu})$. This leads to

$$\zeta^{B4} = 2 - \frac{\mu_O - \mu_P}{\frac{m-\overline{w}}{m\beta(\overline{w})^{1-\alpha}} - \mu_P}, \tag{33}$$

which is the fourth curve from the right side in Fig.6. It is marked with an "S" because it is related to a change in the structure of the map: In the one-dimensional case (i.e. for $\zeta = 1$), the map is continuous on the left side of this line (i.e. it is no longer discontinuous, if we further decrease $\overline{w}$); in the two-dimensional case (i.e. for $\zeta < 1$) the application of $T_L(.)$ and $T_R(.)$ to the line $w_t = \overline{w}$ becomes continuous in the w_t-values (since both functions apply with leftmost branch which is w_t^{α} for both), and the discontinuity is only in the values of μ_t (the jump corresponds to $\mu_{t+1}^R - \mu_{t+1}^L = \zeta(\mu_O - \mu_P)$).

Decreasing $\overline{w}$, the 2-cycle with the symbolic sequence LR still exists, with μ_L and μ_R explicitly given in eq.(25). It undergoes a border collision when the condition $T_R \circ T_L(\overline{w}, \mu_L) = (\overline{w}, \mu_L)$ is satisfied, where $T_R(.)$ applies with Ψ_M^R while $T_L(.)$ applies with w^{α}. This leads to the condition $\overline{w} = \Psi_M^R(\overline{w}^{\alpha}, \mu_R)$, and we get

$$\zeta^{B5} = 2 - \frac{\mu_O - \mu_P}{\frac{m-\overline{w}^{\alpha}}{m\beta(\overline{w})^{\frac{1-\alpha}{\alpha}}} - \mu_P}, \tag{34}$$

which is the fifth bifurcation curve from the right side in Fig.6 colored in red.

For even lower values of $\overline{w}$ the 2-cycle changes structure. A cycle with the symbolic sequence RR, where $T_R(.)$ applies with Ψ_M^R and with w^{α}, related to the flip bifurcation of the fixed point in the R partition, exists, with periodic points belonging to the line $\mu = \mu_O$. Denoting with (w_1, μ_O) and (w_2, μ_O) the two points, the first coordinates of the 2-cycle are implicitly defined by

$$w_1 = \left(\frac{m - w_1}{m\beta\mu_O}\right)^{\frac{\alpha^2}{1-\alpha}} \quad , \quad w_2 = \left(\frac{m - w_0}{m\beta\mu_O}\right)^{\frac{\alpha^2}{1-\alpha}} . \tag{35}$$

For $w_2 = \overline{w}$ this 2-cycle undergoes a BCB. The bifurcation value is independent of ζ, however, no explicit solution exists. This is the sixth curve from the right side in Fig.6, denoted $\overline{w}^{B6}$. With our parameters, this BCB happens at $\overline{w}^{B6} = 0.695$.

As for the previous case, changing the parameters $\overline{w}$ and ζ gives interesting insights into the role of behavioral factors in the stability of the credit market. In this second case μ_O and μ_P are very similar, thus, the transition from a pessimistic to an optimistic credit market sentiment (i.e. crossing $\overline{w}$) has only a weak effect upon the fundamental pledgeability ratio. As in Case 1, the bifurcation diagram in Fig.6 shows that an easier switch to a more optimistic credit market sentiment (a lower $\overline{w}$) stabilizes the net worth evolution with respect to the cycle length. The bifurcation lines are relatively independent of ζ (almost vertical lines in Fig.6), indicating a low influence of ζ. From an economic point of view, this is not so surprising, since in the second case the change in overall credit market sentiment only weakly affects the fundamental value of the pledgeability ratio. Thus, behavioral adjustments – the strength of which are measured by ζ – mostly exert a weak influence.

Again, this assertion needs qualification: for $\zeta < 1$ a parameter region with more complex behavior appears (between two period-2 regions, marked in green in Fig.6(b)) that does not exist for $\zeta = 1$. Thus, also in this case, ζ has a surprising, destabilizing effect that deserves attention. Fig.7(a) shows a one-dimensional bifurcation diagram on ζ in that region (obtained for $\overline{w} = 0.6953$) and reveals the attracting sets and their chaotic structure. It is interesting to note that attracting 2-cycles are never involved.

Note, however, that just outside the green strip in Fig.6(b) the 4-piece chaotic attractor appears to coexist with a 2-cycle, see Fig.7(b) obtained for $\overline{w} = 0.72$, this path is inside the green strip, close to the value $\overline{w}^{B6}$. The two attractors have markedly different amplitudes; thus, a transitory shock (say to the pledgeability ratio) has the potential for substantial long-run effects, it may change the dynamics from a low periodicity with a limited amplitude to a 4-piece chaotic dynamics with a much higher amplitude. Small transitory shocks to the pledgeability ratio may generate regime switches in the time series of net worth: phases of stable dynamics, with small variation in net worth (cycles with low periodicity) alternate with more turbulent phases (larger variation in net worth and chaotic dynamics). As already mentioned, the

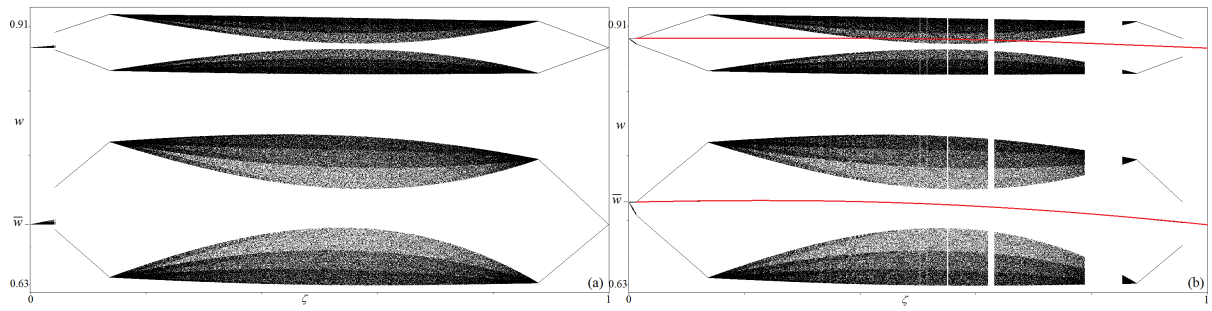

Figure 7: One-dimensional Bifurcation diagrams of w as a function of ζ for $\mu_O = 0.08$. In (a) $\overline{w} = 0.6953$. In panel (b) $\overline{w} = 0.72$. The two-cycle coexisting with the 4-piece chaotic attractor is evidenced in red.

coexistence of attractors introduces also an element of hysteresis; a shock of equal size, but in the opposite direction will not necessarily restore the original situation – an aspect that complicates additionally the resulting time series pattern. These findings are similar to the ones of Schmitt et al. (2017) in a model of market entry and regime switches in the profit taxation function.

5 Conclusion

This paper studies how credit market sentiments affect the long-run stability of a credit cycle model based on Matsuyama et al. (2016). According to our interpretation, the business mood may facilitate or hamper changes in the prevailing credit market sentiment. This is assessed by the current state of the overall economy, proxied by the agents' overall net worth and thus resembling the representativeness heuristic proposed by Kahneman and Tversky (1972). If agents' net worth rises (falls) above (below) a specific threshold (determined by the overall business mood) lenders' perception of the financial friction switch from a pessimistic to an optimistic regime (or vice versa). As a consequence, the pledgeability ratio, which indicates how much of the expected revenue from Bad projects lenders are willing to accept from borrowers as collateral for credit and reflects their attitude towards risk, differs between the regimes.

Before reviewing our results, it might be worthwhile to reflect upon the dynamic processes at work, paying particular attention to the explanation of turning points in the cycles.

Matsuyama's mechanism is the following: Starting with a low net worth, agents are not able to finance Bad projects, as they are not fulfilling the collateral requirement. Investing in Good projects rises the net worth. Eventually, it crosses the relevant threshold and financing Bad projects becomes feasible. Investment into Bad projects is determined by the strength of the pledgeability ratio. Diverting credit from the Good projects reduces the net worth; the cycle reaches a turning point and starts over again. For very high values of the overall net worth the borrowing constraint is no longer binding and financial frictions play no longer a role: It is worth noting that in this case, the (constant) profitability of the Bad projects sets a lower boundary for the investments in Good projects and the returns of Good and Bad projects are equalized.

Our approach introduces a variable pledgeability ratio into this mechanism. An increasing overall net worth eventually crosses the threshold, at which a sudden shift in the agents' assessment about the market mood into the optimistic regime occurs. Agents' perception of the agency problems change and they require less collateral for financing Bad projects - the pledgeability ratio suddenly drops. This leads to a corresponding stronger reaction of the investments in Bad projects. Thus, our behavioral mechanism is expected to amplify cyclical patterns. Good news (the crossing of threshold in upward direction) leads to a more investment in Bad projects; bad news (the crossing of threshold in downward direction) leads to less investments in Bad projects. Note however that it does not add to the explanation of turning points. Note in addition that the amplified cycles make it more likely to hit the lower boundary for investments in Good.

Introducing an endogenous pledgeability ratio links the credit market friction approach to the behavioral explanation of credit market volatility. Our results are in line with findings of recent behavioral explanations of credit cycles. Particularly close is the model by Bordalo et al. (2018). Its core is the operationalization of the representativeness heuristic through diagnostic expectations. This expectation mechanism is their

driving force behind the instability of financial markets. Diagnostic expectations involve an overreaction to news that results in overshooting expectations. Confronted with the actual realization of the states, agents are disappointed; the mechanism reverses and an amplification of the downward movement of the state can be observed. In general, this expectation mechanism creates a boom and bust cycle around credit market fundamentals; this explanation (that includes the turning points) centers on the expectation mechanism. Our model inherits Matsuyama's explanation for the cycles; nevertheless, we obtain similar results as Bordalo et al. (2018) concerning the volatility amplification once the agents assess the market mood resulting in optimistic or pessimistic perception of the agency problems. Note however, compared to Bordalo et al. (2018), the endogenous switching in our setting exerts also a stabilizing element due to the fact that eventually the returns of Good and Bad projects are equalized.

The analytic structure of our model is two-dimensional and only piecewise continuous with a discontinuity stemming from the switch between an optimistic and a pessimistic regime. We implement the regime specific pledgeability ratio according to a mean-reverting dynamic process. This mechanism allows us to take both behavioral inertia and different fundamental values of the pledgeability ratio into account. We presented analytic and simulation results. To facilitate the comparison with Matsuyama et al. (2016) we choose a parameter set that corresponds to chaotic fluctuations in the benchmark model. Our analysis is focused on two cases departing from this framework: in the first case, the difference between the optimistic and pessimistic fundamental perception of the agency problems (parameters μ_P and μ_O) is large; in the second case, this difference is small. For the two cases, we consider the effects of changes in the business mood by variation of the threshold $\overline{w}$ between the optimistic and the pessimistic regime and the degree of behavioral inertia, ζ. While the former acts on the likelihood at which a regime switch may occur, the latter concerns the sluggishness at which the pledgeability ratio is adjusted between the regimes.

In case 1, where the difference between μ_P and μ_O is large, a switch to an optimistic regime corresponds to a substantial change in the fundamental value of the pledgeability ratio. The parameter $\overline{w}$ decreases below unity, and thus allows for a switch towards an optimistic regime indicating an improvement in the business mood. Overall, we find that this leads to a transition from chaotic fluctuations to cycles with finite periodicity.

Therefore, at first glance, the introduction of credit market sentiments stabilizes the economy by dampening the more erratic and turbulent behavior. However, we also observe that the amplitude of those periodic cycles is higher, adding an additional element of volatility to agents' net worth fluctuations. Moreover, the frequency of switching between the perception of the credit market frictions also increases.

By reducing $\overline{w}$ further, the stabilizing effect of more optimism becomes obvious through a declining periodicity of the cycles, eventually converging to a fixed point solution. Hence, the economy converges to a stationary equilibrium. The economic rationale behind this surprising result is the following: In the benchmark framework, a low pledgeability ratio reflects a high degree of credit market imperfections. Thus, allowing a switch to an optimistic regime, which involves a higher pledgeability ratio, actually reduces credit market imperfections and exerts a stabilizing effect.

Moreover, we have seen that adding behavioral inertia (ζ) to the adjustment of the pledgeability ratio has an impact on cycles periodicity. Starting from a value of $\overline{w}$ corresponding to periodic fluctuations, phases of increasing and decreasing periodicity are alternating. This phenomenon also affects the average net worth, which increases during the phases of period adding. In fact, the effect of behavioral inertia adds another element of complexity to the system.

In case 2, the difference between μ_P and μ_O is small such that a switch to an optimistic regime leads only to a minor change in the fundamental value of the pledgeability ratio. In this scenario the impact of a reduction of $\overline{w}$ is similar to the previous case as we observe a stabilizing effect through a reduction of periodicity while at the same time extending the amplitude. Adding behavioral inertia has a predominantly small impact on the dynamics as μ_P and μ_O are very close. However, for intermediate values of $\overline{w}$ and ζ, chaotic fluctuations emerge which confirms a destabilizing effect of behavioral inertia.

Finally, we observe regions where attractors coexist and may differ quite substantially. For example, in the second scenario, an attractor with a rather low frequency and a limited amplitude coexists with a four-piece chaotic attractor with a much higher amplitude. Thus, (transitory) exogenous shocks to the net worth or to the pledgeability ratio may produce quite different trajectories that may involve periods with high volatility. Thus, our model is able to reproduce the stylized fact of volatility clustering which is quite common in economic and financial time series.

In summary, our results confirm the view of the literature on behavioral finance, according to which the business mood and switches in agents' beliefs explain the widening of credit cycle fluctuations. Compared to the baseline model, the possibility to switch to an optimistic perception reduces financial frictions which stabilizes the system. The erratic and turbulent behavior of the net worth evolution is eliminated. However, at the same time a destabilization occurs since the amplitude of cycles is increased and thus volatility is more evident.

Acknowledgement: The authors thank two anonymous referees for the careful reading and the valuable suggestions; and the participants of the 2017 NED conference in Pisa and the 2018 MDEF conference in Urbino for helpful comments and suggestions; and Ebony Granada for valuable editorial support. Ingrid Kubin and Thomas O. Zörner gratefully acknowledge financial support from the Austrian National Bank, Jubilaeumsfond grant no. 16748.

6 References

1. Baker, M. & Wurgler, J. (2007), 'Investor Sentiment in the Stock Market', Journal of Economic Perspectives 21(2), 129–152.

2. Baron, M. & Xiong, W. (2017), 'Credit expansion and neglected crash risk', The Quarterly Journal of Economics 132(2), 713–764.

3. Bernanke, B. & Gertler, M. (1989), 'Agency costs, net worth, and business fluctuations', American Economic Review 79(1), 14–31.

4. Bordalo, P., Gennaioli, N. & Shleifer, A. (2018), 'Diagnostic expectations and credit cycles', The Journal of Finance 73(1), 199–227.

5. Brunnermeier, M. K. & Sannikov, Y. (2014), 'A macroeconomic model with a financial sector', American Economic Review 104(2), 379–421.

6. Campisi, G., Naimzada, A. & Fabio Tramontana (2018), 'Local and global analysis of a speculative housing market with production lag', Chaos 28.

7. Chiarella, C., Guilmi, C. D. & Zhi, T. (2015), Modelling the animal spirits of bank's lending behavior, Working paper series, Finance Discipline Group, UTS Business School, University of Technology, Sydney.

8. Commendatore, P., Kubin, I., Mossay, P. & Sushko, I. (2017), 'The role of centrality and market size in a four-region asymmetric new economic geography model', J Evol Econ 27, 1095–1131.

9. Day, R. & Huang, W. (1990), 'Bulls, bears and market sheep', Journal of Behavior & Organization 14, 299–329.

10. DeLuigi, C. & Huber, F. (2018), 'Debt regimes and the effectiveness of monetary policy', Journal of Economic Dynamics and Control 93, 218-238.

11. Diamond, P. (1965), 'National debt in a neoclassical growth model', American Economic Review 55, 1126–1150.

12. Edwards, W. (1968), Conservatism in human information processing, in B. Kleinmutz (Ed.), Formal Representation of Human Judgment, John Wiley and Sons, New York, pp. 17-52.

13. Favara, G. (2012), 'Agency problems and endogenous investment fluctuations', The Review of Financial Studies 25(7), 2301–2342.

14. Franke, R. (2008), 'A microfounded herding model and its estimation on german survey expectations', European Journal of Economics and Economic Policies: Intervention 5(2), 301–328.

15. Franke, R. & Westerhoff, F. (2017), 'Taking stock: A rigorous modeling of animal spirits in macroeconomics', Journal of Economic Surveys 31(5), 1152–1182.

16. Frankel, J. A. & Froot, K. A. (1987), 'Using survey data to test standard propositions regarding exchange rate expectations', American Economic Review 77(1), 133–153.

17. Frankel, J. A. & Froot, K. A. (1990), 'Chartists, fundamentalists, and trading in the foreign exchange market', American Economic Review 80(2), 181–185.

18. Gao, L. & Suess, S. (2015), 'Market sentiment in commodity futures returns', Journal of Empirical Finance 33, 84 – 103.

19. Gennaioli, N. & Shleifer, A. (2018), A Crisis of Beliefs, Princeton University Press.

20. Grauwe, P. D. & Macchiarelli, C. (2015), 'Animal spirits and credit cycles', Journal of Economic Dynamics and Control 59, 95 – 117.

21. Hommes, C. (2006), Heterogeneous agent models in economics and finance, in L. Tesfatsion & K. L. Judd, eds, 'Handbook of Computational Economics', Vol. 2 of Handbook of Computational Economics, Elsevier, chapter 23, pp. 1109–1186.

22. Hotz-Behofsits, C., Huber, F. & Zörner, T. O. (2018), 'Predicting crypto-currencies using sparse non-gaussian state space models', Journal of Forecasting 37 (6), 627-640.

23. Huber, F. & Zörner, T. O. (2019), Threshold cointegration in international exchange rates: A Bayesian approach, International Journal of Forecasting 35 (2), 458-473.

24. Kahneman, D., & Tversky, A. (1972), 'Subjective probability: A judgment of representativeness', Cognitive Psychology 3, 430-454.

25. Keynes, J. M. (1936), The General Theory of Employment, Interest and Money, Macmillan:London.

26. Kiyotaki, N. & Moore, J. H. (1997), 'Credit cycles', Journal of Political Economy 105, 211–248.

27. Lamantia, F. & Radi, D. (2018), 'Evolutionary technology adoption in an oligopoly market with forward-looking firms', Chaos 28.

28. Lopez-Salido, D., Stein, J. C. & Zakrajsek, E. (2017), 'Credit-market sentiment and the business cycle', The Quarterly Journal of Economics 132(3), 1373–1426.

29. Lux, T. (2009), 'Rational forecasts or social opinion dynamics? Identification of interaction effects in a business climate survey', Journal of Economic Behavior & Organization 72(2), 638– 655.

30. Matsuyama, K. (2008), 'Aggregate implications of credit market imperfections', NBER Macroeconomics Annual 22, 1–49.

31. Matsuyama, K. (2013), 'The good, the bad, and the ugly: An inquiry into the causes and nature of credit cycles', Theoretical Economics 8, 623–651.

32. Matsuyama, K., Sushko, I. & Gardini, L. (2016), 'Revisiting the model of credit cycles with good and bad projects', Journal of Economic Theory 163, 525–556.

33. Mendoza, E. G. & Terrones, M. E. (2008), An Anatomy Of Credit Booms: Evidence From Macro Aggregates And Micro Data, NBER Working Papers 14049, National Bureau of Economic Research.

34. Minsky, H. P. (1982), The financial instability hypothesis: Capitalistic processes and the behavior of the economy, in: Kindleberger, C.P, Laffargue, J.P. (Eds.), Financial Crisis: Theory, History, and Policy', Cambridge University Press, Cambridge, 13–29.

35. Nofsinger, J. R. (2005), 'Social mood and financial economics', Journal of Behavioral Finance 6(3), 144–160.

36. Radi, D. & Gardini, L. (2015), 'Entry limitations and heterogeneous tolerances in a Schelling-like Segregation Model', Chaos Solitons & Fractals 79, 130–144.

37. Schmitt, N., Tuinstra, J. and Westerhoff, F. (2017): 'Side effects of nonlinear profit taxes in a behavioral market entry model: abrupt changes, coexisting attractors and hysteresis problems', Journal of Economic Behavior and Organization 135, 15-38.

38. Schularick, M. & Taylor, A. M. (2012), 'Credit booms gone bust: Monetary policy, leverage cycles, and financial crises, 1870-2008', American Economic Review 102(2), 1029–61.

39. Shiller, R.J. (2003), 'From Efficient Markets Theory to Behavioral Finance', The Journal of Economic Perspectives 17(1), 83-104.

40. Shleifer, A. (2000), Inefficient markets: An introduction to behavioural finance, Oxford University Press.

41. Shu, H. C. (2010), 'Investor mood and financial markets', Journal of Economic Behavior & Organization 76(2), 267-282.

42. Sushko, I., Gardini, L. & Matsuyama, K. (2014), 'Superstable credit cycles and U-sequence', Chaos Solitons & Fractals 59, 13–27.

43. Sushko, I., Gardini, L. & Matsuyama, K. (2018), 'Coupled Chaotic Fluctuations in a Model of International Trade and Innovation: Some Preliminary Results', Communications in Nonlinear Science and Numerical Simulation 58, 287–302.

44. Thaler, R., (2003), Advances in Behavioral Finance II, Russel Sage, New York.

45. Tirole, J. (2005), The Theory of Corporate Finance, Princeton University Press.

46. Tramontana, F., Westerhoff, F. & Gardini, L. (2013), 'The bull and bear market model of Huang and Day: Some extensions and new results', Journal of Economic Dynamics & Control 37, 2351–2370.

47. Tramontana, F., Gardini, L. & Puu, T. (2010), 'Global Bifurcations in a Piecewise-Smooth Cournot Duopoly Game', Chaos, Solitons & Fractals 43, 15–24.

48. Tramontana, F., Gardini, L. & Puu, T. (2011), 'Mathematical Properties of a combined Cournot-Stackelberg model', Chaos, Solitons & Fractals 44, 58–70.

7 APPENDIX

7.1 Appendix: Bifurcation analysis of the 2-cycle in Fig.2

Although a 2-cycle with periodic points in the same region of the map is possible (see the cycle with symbolic sequence RR in Sec.4.2), those observed in Fig.2(a) all involve one periodic point in each of the two regions L/R of the map. Let us denote the points of such a 2-cycle with (w_L, μ_L) and (w_R, μ_R) satisfying $T_L(w_L, \mu_L) = (w_R, \mu_R)$ and $T_R(w_R, \mu_R) = (w_L, \mu_L)$. These periodic points are fixed points of the second iterate of the map, which still is in triangular form. Therefore, the Jacobian matrix at a 2-cycle of this kind is given by $J_{T_L}(w_L, \mu_L) J_{T_R}(w_R, \mu_R)$:

$$\begin{bmatrix} \frac{\partial}{\partial w}\Psi_M^L(w_L,\mu_L)\frac{\partial}{\partial w}\Psi_M^R(w_R,\mu_R) & \frac{\partial}{\partial \mu}\Psi_M^L\frac{\partial}{\partial \mu}\Psi_M^R + \frac{\partial}{\partial \mu}\Psi_M^L(1-\zeta) \\ 0 & (1-\zeta)^2 \end{bmatrix} \tag{36}$$

and when existing the 2-cycle is either locally attracting or a saddle.

From the triangular structure the second component of the 2-cycle can easily be obtained explicitly. From $T_L(w_L, \mu_L) = (w_R, \mu_R)$ and $T_R(w_R, \mu_R) = (w_L, \mu_L)$ we have

$$\mu_R = (1-\zeta)\mu_L + \zeta\mu_P \quad , \quad \mu_L = (1-\zeta)\mu_R + \zeta\mu_O \tag{37}$$

from which

$$\mu_R = \mu_O - \frac{\mu_O - \mu_P}{2-\zeta} \quad , \quad \mu_L = \mu_P + \frac{\mu_O - \mu_P}{2-\zeta} \tag{38}$$

and

$$w_R = \begin{cases} w_L^{\alpha} & if \quad w_L \le w_c^L \\ \Psi_M^L(w_L, \mu_L) = \left(\frac{m-w_L}{m\beta\mu_R}\right)^{\frac{\alpha}{1-\alpha}} & if \quad w_c^L \le w_L \le m(1-\mu_R) \\ \widehat{\beta} & if \quad w_L \ge m(1-\mu_R) \end{cases} \tag{39}$$

$$w_L = \begin{cases} w_R^{\alpha} & if \quad w_R \le w_c^R \\ \Psi_M^R(w_R, \mu_R) = \left(\frac{m-w_R}{m\beta\mu_L}\right)^{\frac{\alpha}{1-\alpha}} & if \quad w_c^R \le w_R \le m(1-\mu_L) \\ \widehat{\beta} & if \quad w_R \ge m(1-\mu_L) \end{cases} \tag{40}$$

which exists iff $w_R > \overline{w}$ and $w_L < \overline{w}$. At $w_R = \overline{w}$ and $w_L = \overline{w}$ the 2-cycle appears/disappears via a BCB, and we provide explicit conditions for these bifurcations to occur.

A first possible 2-cycle is with periodic points $w_L = \widehat{\beta}$ and $w_R = (\widehat{\beta})^{\alpha}$ and the related BCBs occur for $\overline{w} = \widehat{\beta}$ and $\overline{w} = (\widehat{\beta})^{\alpha}$, respectively (vertical black lines in Fig.2(a,b), where $\widehat{\beta} < (\widehat{\beta})^{\alpha}$).

Another 2-cycle involves the periodic points $w_R = \Psi_M^L(w_L, \mu_L)$ and $w_L = \Psi_M^R(w_R, \mu_R)$. We have not an explicit solution for the BCB that occus at the collision with $\overline{w}$, thus the curves are detected numerically in the following way: Fixing a value of ζ determines the corresponding values for μ_L and μ_R (see eq.(38)).

A first BCB occurs for $w_L = \overline{w}^{BCB1}$, thus,

$$\overline{w}^{BCB1} = \left(\frac{m-w_R}{m\beta\mu_L}\right)^{\frac{\alpha}{1-\alpha}} \quad , \quad \text{where} \quad w_R = \left(\frac{m-\overline{w}^{BCB1}}{m\beta\mu_R}\right)^{\frac{\alpha}{1-\alpha}} , \tag{41}$$

holds (μ_R and μ_L are as given in eq.(38)). Solving for $\overline{w}^{BCB1}$ (for each value of ζ) results in the related bifurcation line.

A second BCB occurs for $w_R = \overline{w}^{BCB2}$, thus,

$$\overline{w}^{BCB2} = \left(\frac{m-w_L}{m\beta\mu_R}\right)^{\frac{\alpha}{1-\alpha}} \quad , \quad \text{where} \quad w_L = \left(\frac{m-\overline{w}^{BCB2}}{m\beta\mu_L}\right)^{\frac{\alpha}{1-\alpha}} , \tag{42}$$

holds (here also μ_R and μ_L are as given in eq.(38)) and a second bifurcation line can be determined. The two curves are evidenced in Fig.2(a,b) for low values of ζ.

From the figures we have evidence that the existence regions of a stable fixed point and a stable 2-cycle are overlapping, so that we have regions of coexistence.

7.2 Appendix: Determination of the bifucation value $\overline{w}^{Bif}$ and discussion

We consider here the transition between the chaotic interval and cycles with high periodicity. Fig.8 depicts the phase space and illustrates this transition: The critical line LC_{-1} is the locus of points w_c^L; it intersects the line $\mu = \mu_P$ in the critical point C_{-1} (point of the local maximum for the one-dimensional function $\Psi_M^L(w, \mu)$). The other two curves, LC and LC_1, and the other two points, C and C_1, are the images. In Fig.8(a) at $\overline{w} = 0.955$ it is $C < \overline{w}$ and the attracting (chaotic) set is still on the line $\mu = \mu_P$. Note that for high values of $\overline{w}$ (close to $\overline{w} = 1$) the map has a saddle fixed point (w^{*L}, μ_P) with $w^{*L} = 0.8825$ which is transversely attracting and whose local unstable set is on the line $\mu = \mu_P = 0.05$ (on which the restriction of the map is one-dimensional). Therefore, the chaotic interval $[C_1, C]$ - which is bounded by two critical points - is attracting for map T as long as it is on the left side of the line $w = \overline{w}$. The bifurcation occurs when this chaotic segment has a contact with the line $w = \overline{w}$, that is, when the critical point touches that line, at $C = \overline{w}$.

This bifurcation can be determined in implicit form: First, we determine the point C_{-1}, at which the critical line LC_{-1} intersects the μ_P line. Its coordinates are denoted by $(\widetilde{w}, \mu_P)$ and $\widetilde{w}$ is the solution to (using the definition, the intersection point of the two branches of the function defining T_L):

$$\left(\frac{m-\widetilde{w}}{m\beta\left((1-\zeta)\mu_P + \zeta\mu_P\right)}\right)^{\frac{\alpha}{1-\alpha}} = (\widetilde{w})^{\alpha}$$

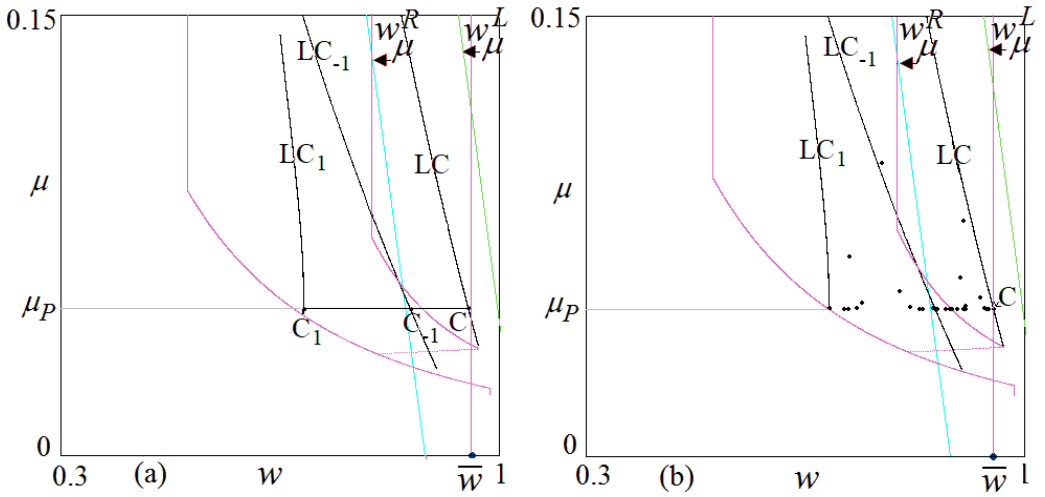

Figure 8: Attractors for $\mu_O = 0.4$ and $\zeta = 0.4$. In (a) $\overline{w} = 0.955 > \overline{w}^{Bif}$. In (b) $\overline{w} = 0.95 < \overline{w}^{Bif}$. The line $w = \overline{w}$ separates the two partitions where the functions T_L and T_R apply.

that is:

$$\left(\frac{m - \widetilde{w}}{m\beta\mu_P}\right)^{\frac{1}{1-\alpha}} = \widetilde{w}$$

Note that this value $\widetilde{w}$ depends only on μ_P (i.e. it is independent of ζ and of μ_O). Then, the critical point C is obtained as image of the point $\widetilde{w}$, leading to $C = (\widetilde{w}^\alpha, \mu_P)$. At $\overline{w}^{Bif} = \widetilde{w}^\alpha$ the bifurcation occurs, and the bifurcation value is independent of ζ and of μ_O.

This bifurcation involves the transition from an attracting set only on the L side and on the line $\mu = \mu_P$ (a chaotic interval in Fig.8(a)) to an attracting set of the plane. This attracting set in general is a superstable cycle involving the point $\left(\widehat{\beta}, \widehat{\mu}\right)$, where $\widehat{\mu} = (1-\zeta)\mu_P + \zeta\mu_O$.

Fig.8(b) is drawn for $\overline{w} = 0.95$ (i.e. $C > \overline{w}$) and depicts a situation soon after the bifurcation. Since the right part of the map (with the function $T_R(w_t, \mu_t)$) comes to play a role in the limit set of the trajectories, the attracting set has now points also outside the line $\mu = \mu_P$. For the chosen parameters (implying a rather low w_μ^R) the map on the right side is $w_{t+1}^R = \widehat{\beta}$ and this explains the appearance of a superstable cycle. In fact, the Jacobian matrix on the right side related to the flat branch has eigenvalues 0 and $(1-\zeta)$. Thus when a cycle appears of some period $n > 1$ it is always superstable, since the map T^n is in triangular form with one eigenvalue equal to 0 and another one given by $(1-\zeta)^n$.

This is well observable in the two-dimensional bifurcation diagram in Fig.2(a,c), where the vertical line at $\overline{w}^{Bif}$ indicates this bifurcation and shows the sharp transition from a chaotic set on the line $\mu = \mu_P = 0.05$ to an attracting cycle of the plane.

7.3 Appendix: Determination of the bifurcation value ζ^{Bif} and discussion

The effect of varying ζ at a fixed value of $\overline{w}$ is shown in Fig.4(a,b), representing the path along the blue line in Fig.2(c). We can see that there are superstable cycles with the periodic point $\left(\widehat{\beta}, \widehat{\mu}\right)$ (where $\widehat{\mu} = (1-\zeta)\mu_P + \zeta\mu_O$ as given in (27)). Interestingly, at very low values of ζ the periodicity of the superstable cycles increases. Decreasing ζ the transition from superstable cycles to a two-dimensional attracting set that may be chaotic occurs, at a bifurcation value denoted ζ^{Bif}. Notice that decreasing the value of ζ the straight line w_μ^R moves more on the right side of the attractor, which is still a cycle with increasing period (an example is shown in Fig.9(a)). The bifurcation occurs when the invariant area has a tangency contact point with the border line w_μ^R. Before this bifurcation, the invariant area intersects the line w_μ^R in two distinct points (as in Fig.9(a)). At the bifurcation, the two points merge; and after the bifurcation the invariant area

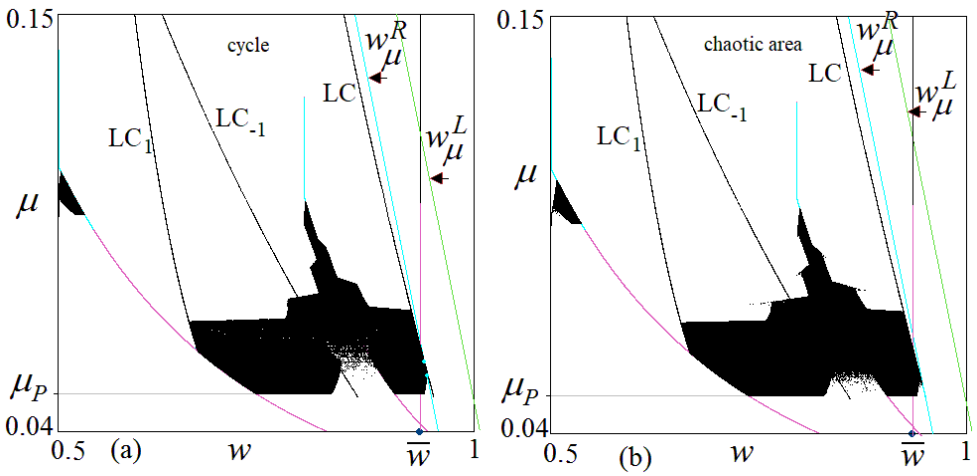

Figure 9: Attractors for $\overline{w} = 0.935$ and $\mu_O = 0.4$. In (a) $\zeta = 0.135$. In (b) $\zeta = 0.13$.

has no contact with the border line. This means that the branch of T_R involved is no longer flat, and the attracting set becomes a chaotic area completely on the left side of the border line, as shown in Fig.9(b). That is, before the bifurcation the flat branch of the function T_R is involved and $\left(\widehat{\beta}, \widehat{\mu}\right)$ is a periodic point, after the bifurcation the flat branch of the function T_R is no longer involved.

The transition described above occurs when the critical point $C = (\widetilde{w}^\alpha, \mu_P)$ merges with the point of intersection of $w_\mu^R = m(1 - ((1-\zeta)\mu + \zeta\mu_O))$ with the line $\mu = \mu_P$, leading to

$$\widetilde{w}^\alpha = m(1 - \mu_P - \zeta\,(\mu_O - \mu_P)).$$

Since $\widetilde{w}$ is independent of ζ (and of μ_O), this equation can be solved for ζ giving:

$$\zeta^{Bif} = \frac{m\,(1-\mu_P) - \widetilde{w}^\alpha}{m\,(\mu_O - \mu_P)}.$$

Note that a decreasing μ_O increases this threshold value.

7.4 Appendix: Bifurcation structure decreasing ζ

Varying ζ changes the definition of the two-dimensional map in the middle branches in eq.(12). Let us here describe some bifurcations occurring at fixed value of $\overline{w}$ and decreasing ζ as shown in Fig.2(c) and Fig.4(a,b).

For $\zeta = 1$ as well as for lower values of ζ, in the L side of the map, i.e. for $w < \overline{w}$, there exists a repelling fixed point (w^{*L}, μ_P) and a repelling 2-cycle (flip bifurcated from that fixed point) on the line $\mu = \mu_P$. At $\zeta = 1$ there exists an attracting 15-cycle with symbol sequence $LL(MLML)^3R$ that involves the point $(w_1, \mu_1) = (\widehat{\beta}, \widehat{\mu})$ where $\widehat{\mu} = (1-\zeta)\mu_P + \zeta\mu_O$, as given in equation (27), and notice that this decreases when decreasing ζ. Here we denote with L/M the left and right side with respect to the critical point w_c^L of map T, and R corresponds to the right side of $\overline{w}$ where the function T_R applies with the flat branch (i.e. where the points are mapped into $\widehat{\beta}$). Because of space limitations, we do not present a comprehensive discussion of the bifurcation scenario on $\overline{w}$ at $\zeta = 1$.

Decreasing ζ the existing cycle involves the periodic point $(w_1, \mu_1) = (\widehat{\beta}, \widehat{\mu})$ and relevant is the pre-image of this periodc point, which is the periodic point of the cycle on the right side, i.e. $w_{15} > \overline{w}$, and it is the only periodic point of the cycle on the right side of the border (as it is for $\zeta = 1$), so the point is $(w_{15}, \mu_{15}) = (w_{15}, \mu_P) = (w_{15}, 0.05)$. The first periodic point, which is always $(w_1, \mu_1) = (\widehat{\beta}, \widehat{\mu})$ (in the upper left side in in Fig.10), and the last periodic point (in the lower right side in Fig.10) are evidenced by arrows, showing the points of the cycle.

Fig.10(a), for $\zeta = 0.9$, shows that the periodic points of symbolic sequence $LL(MLML)^3R$ and decreasing ζ the point (w_{11}, μ_{11}) approaches the border, the BCB occurs when $w_{11} = \overline{w}$ after which the periodic point

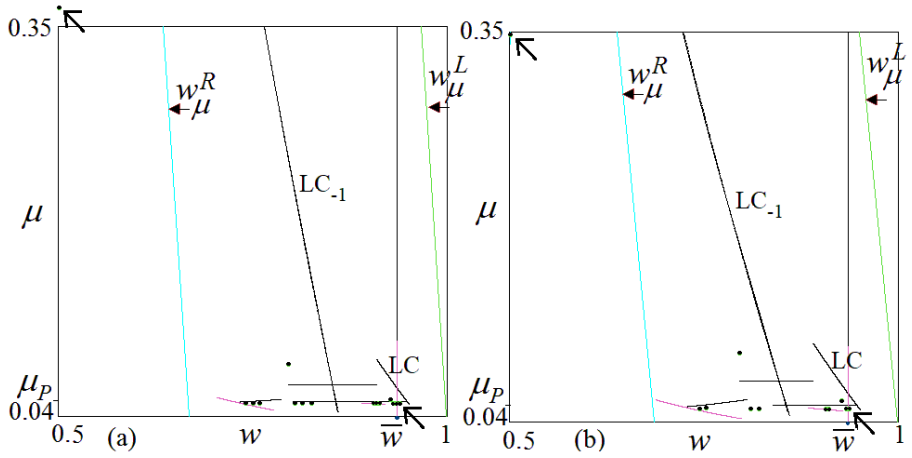

Figure 10: Attractors for $\overline{w} = 0.935$ and $\mu_O = 0.4$. In (a) $\zeta = 0.9$. In (b) $\zeta = 0.85$.

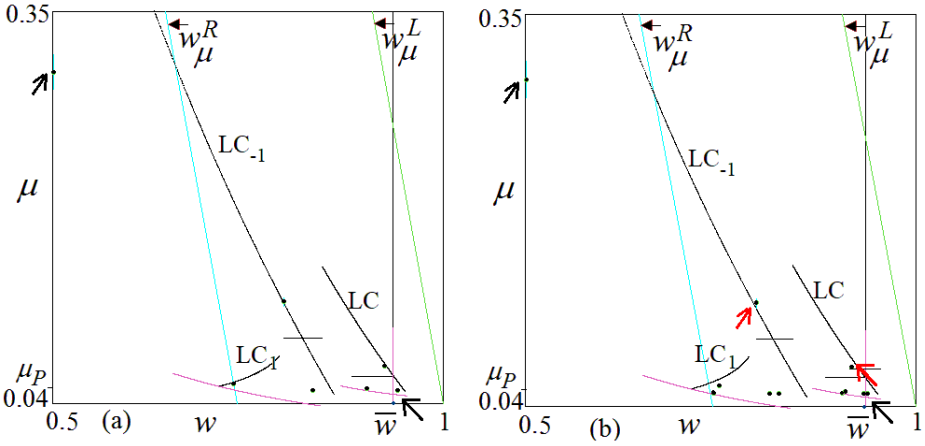

Figure 11: Attractors for $\overline{w} = 0.935$ and $\mu_O = 0.4$. In (a) $\zeta = 0.72$. In (b) $\zeta = 0.71$.

enters the R region and now it will take 4 iterations less than before to reach again the R side, leading to a 11-cycle with symbolic sequence $LL(MLML)^2R$ (shown in Fig.10(b) for $\zeta = 0.85$). Decreasing ζ the same process repeats and the point (w_7, μ_7) approaches the border, the BCB occurs when $w_7 = \overline{w}$ after which the periodic point enters the R region and now it will take 4 iterations less than before to reach again the R side, leading to a 7-cycle with symbolic sequence $LL(MLML)R$ (shown in Fig.11(a), for $\zeta = 0.72$).

From now on, decreasing ζ, the two-dimensional structure of the map plays a central role, the periodic points of the cycle are in fact on the right and left sides of the segments belonging to the local stable set of the unstable 2-cycle on $\mu = \mu_P$. At $\zeta = 0.712$ close to the BCB the last periodic point of the 7-cycle (w_7, μ_7) with $w_7 > \overline{w}$, is very close to the boundary, at the bifurcation $w_7 = \overline{w}$ the periodic point $(w_1, \mu_1) = (\widehat{\beta}, \widehat{\mu})$ has the first two images closer to the unstable set of the 2-cycle (evidenced by red arrows in Fig.11(b)), which means that the trajectory take 4 iterations more to reach the R side, leading to an 11-cycle, always with a unique, last, point in the R side (an example in Fig.11(b) for $\zeta = 0.71$). This process is repeated ad infinitum, for all cycles of odd periods $LL(MLML)^nR$, $n > 1$, for each cycle the last periodic point undergoes a BCB with $\overline{w}$ decreasing ζ and its images are closer and closer to the stable set of the 2-cycle. At each bifurcation the period is increased by 4 units. A finite value of ζ exists at which the image of $(w_1, \mu_1) = (\widehat{\beta}, \widehat{\mu})$ belongs to the stable set of the 2-cycle, leading to a Milnor attractor, this is the center of the "spider structure", indicated by an arrow in Fig.4. After the Milnor attractor, the image of $(w_1, \mu_1) = (\widehat{\beta}, \widehat{\mu})$ is on the other side of the stable set of the 2-cycle, leading (decreasing ζ) to cycles whose periods are now decreasing by 4 units at each BCB (in a reverse process similar to the forward one, the images of $(w_1, \mu_1) = (\widehat{\beta}, \widehat{\mu})$ are mapped

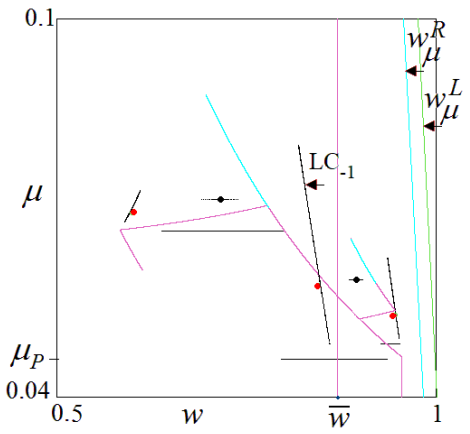

Figure 12: Attractors for $\alpha = 0.33$, $m = 1.05$, $B = 2$, $\overline{w} = 0.87$, $\mu_P = 0.05$, $\mu_O = 0.08$, $\zeta = 0.6$.

farther from the stable set of the 2-cycle).

A similar process is repeated several times, as shown in Fig.4(a,b), leading to several "spider structures", whose bifurcation mechanism, described above, has been also described in other papers, see for example Tramontana et al. (2010,2011) and Sushko et al. (2014).

7.5 Appendix: Bifurcation analysis of the 3-cycle in Fig.6(a)

In Fig.12, which illustrates this argument, the attracting 3-cycle (red points) coexists with the attracting 2-cycle (black points), and one periodic point is close to LC_{-1}. Decreasing ζ this periodic point crosses LC_{-1} so that even if the cycle is still with two periodic points on the left side and one point on the right side, now one branch of the left side is applied with w^α and the second one with Ψ^L_M which has a larger eigenvalue leading to a saddle 3-cycle.[16] This transition to an unstable 3-cycle also leads to the appearance of chaotic dynamics.

[16] Also 3-cycles may exist that are determined by the condition $T_L \circ T^2_R(\overline{w}) = \overline{w}$ where $T_R(.)$ applies with Ψ^R_M while $T_L(.)$ applies with w^α. In that case, the points cannot be obtained in explicit form; and probably this cycle is unstable since the eigenvalue different from $(1-\zeta)$ of the point on the right side is larger than 1 in modulus.